DYNAMIC RISK ANALYSIS OF OFFSHORE FACILITIES IN HARSH ENVIRONMENTS

by

© Jinjie Fu

A thesis submitted to the

School of Graduate Studies

in partial fulfillment of the requirement for the degree of

Master of Engineering

Faculty of Engineering and Applied Science

Memorial University of Newfoundland

May 2020

St. John's Newfoundland and Labrador

Abstract

With the frequent occurrence of extreme weather conditions, the safe operation of offshore facilities has been seriously challenged. Previous research attempted to simulate hydrodynamic performance or structure dynamic analysis to single environmental load. The present thesis proposes two methodologies to assess the operational risk quantitatively with combined wind and wave loads in a harsh environment considering the dependence structure between the real-time environmental parameters.

The first developed model calculates the environmental loads using wind load response modeling, the Morison model and the ultimate limit states method. Then physical reliability models and joint probability functions derive the probabilities of failure at the level of structural components corresponding to combined loads. BN integrates the root probabilities according to the unit configuration to calculate the failure probability of the Semi-submersible Mobile Unit (SMU). The model is examined with a case study of the Ocean Ranger capsizing accident on Feb 15, 1982. The model uses the prevailing weather conditions and calculates a very high probability of failure 0.7812, which proves the robustness and effectiveness of the proposed model.

The second proposed model is the copula-based bivariate operational failure assessment function, which assesses the dependencies among the real-time environmental parameters. Dependence function is described by the parameter δ from the wave data and concurrent meteorological observation data which are obtained from the Department of Fisheries and Oceans Canada (DFO). Then, the true model is selected with the help of Akaike's information criterion (AIC)

differences and Akaike weight. Comparing the results from the proposed approach and the traditional approach, it is shown that operational failure probabilities considering dependence are noteworthy higher and deserve attention. In other words, the traditional approach underestimates the operational risk of offshore facilities, especially in harsh environments.

Keywords: Operational failure; Semi-submersible mobile unit; Physical reliability model; Dependence; Copula function; Bayesian network; Environmental loads

Acknowledgements

Studying at the Memorial University of Newfoundland with my supervisor Dr. Faisal Khan is an unforgettable and wonderful period in my life. His excellent attitude and rich academic background deeply impress me every time when we discuss the research problems. In the academy, his meticulous attitude and high standards urge me to keep forward. In life, he is more like a father, always advising me on where my life should head to at the right time. I really appreciate him for the patient guidance in the past two years of graduate study.

I also thankfully acknowledge the financial support from the Natural Science and Engineering Council of Canada (NSERC) and the Canada Research Chair (CRC) Tier I Program in Offshore Safety and Risk Engineering. I would like to thank Chuanqi Guo and Guozheng Song, Ruochen Yang, and Xi Chen and all the research fellows of Centre for Risk, Integrity, and Safety Engineering (C-RISE) for their encouragement and constructive suggestions.

I am grateful to Daqian Zhang and Fan Zhang, Jin Gao and other friends, who accompany and motivate me all the time in St. John's. They make me feel that life is colorful and full of sunshine. Last but not least, I am indebted to my beloved parents for their love, constant support and encouragement. It is they who have cheered me up and helped me through the hard times during the past twenty-four years. Sureness, confidence, and kindness are the most important gifts they give me. I dedicate this work to them.

Table of Contents

List of Tables

List of Figures

List of Abbreviations

ABS	American Bureau of Shipping
AIC	Akaike's Information Criterion
BN	Bayesian Network
BT	Bow-tie
CBBN	Copula-based Bayesian Network
CML	Canonical Maximum Likelihood
COV/CV	Coefficient of Variation
CPT	Conditional Probability Table
DFO	Department of Fisheries and Oceans
DRA	Dynamic Risk Assessment
EML	Exact Maximum Likelihood
ETA	Event Tree Analysis
FSU	Floating Storage Unit
FTA	Fault Tree Analysis
IFM	Inference Functions for Margins
IMS	Improved Mixture Simulation
LLF	Log-likelihood Function
MODU	Mobile Offshore Drilling Unit
NOAA	National Oceanic and Atmospheric Administration
PDF	Probability Density Function
PoF	Probability of Failure

QRA	Quantitative Risk Assessment
SMU	Semi-submersible Mobile Unit
TLP	Tension Leg Platform
USNRC	United State Nuclear Regulatory Commission

Co-authorship Statement

Jinjie Fu is the principal author of all the papers presented in the thesis. My supervisor Dr. Faisal Khan identified the research gap and assisted Jinjie Fu to determine the research topic. Then Jinjie Fu conducted an extensive literature review and proposed related methodologies aiming to analysis operational risk in terms of the combined environmental loads. Dr. Faisal Khan provided a solid theoretical orientation in the research process. Furthermore, the calculation and discussion of the results were finished by Jinjie Fu under the direct supervision of Dr. Faisal Khan. Jinjie Fu prepared and revised the drafts of manuscripts based on the suggestions of co-author Dr. Faisal Khan and the feedback from peer review.

Chapter 1. Introduction and Overview

As the source power of economic growth, energy plays a crucial role in national living and industrial production, among which oil and natural gas occupy a significant proportion. Offshore oil and gas reservoirs are increasingly attracting people's attention from conventional land-based reservoirs well drilling and production to offshore hydrocarbon exploration and exploitation. However, it is worth noting that the fickle and inclement ocean weather seriously threatens the safe operation of the offshore facilities [1-2]. For instance, it reveals that the 2005 Atlantic hurricane season was the most active of record which includes the most number of tropical storms (28) and the most number of hurricanes (15) according to the annual summary from NOAA [3]. A tremendous amount of drilling and production platforms were damaged or destroyed by hurricanes [4]. Therefore, the rigorous situation underscores the urgent need for a suitable model to assess the operational failure to guide and coordinate safety production.

1.1 Research on the evaluation impact of the environmental loads

To study the impact on the offshore facilities of the environmental loads, many previous attempts have been conducted. Guan et al. [5] combined the finite element method and wind field test to assess the derrick stress concentration of an offshore module drilling rig under wind loads. Bea et al. [6] proposed an integrated approach using the Morison model to calculate the wave impact loads on the deck, validated by laboratory tests. Lee et al. [7] studied the derrick performance considering gravity and wind pressure, based on the backpropagation

neural network (BPN) for accuracy and efficiency. However, these studies lack the investigation of the impact of environmental loads on offshore facilities as a whole system rather than one individual structural component.

Furthermore, field tests, experimental studies, and numerical simulations have been developed to analyze the influence of a specific load. With the aid of wind tunnel tests, Zhai et al. [8] measured the wind pressure distribution on a 1/100 scale model of HYSY-981. Gonçalves et al. [9] presented the experimental study of motion amplitudes of a semi-submersible platform under the impact of regular and irregular waves. Liu et al. [10] conducted an assessment of acceleration and displacement response for towering structures of an offshore oil platform caused by fluctuating wind loads. Lee et al. [11] used CFD to simulate the dynamic air-gap and wave-imposed loads, based on the JONSWAP spectrum irregular wave profile. While the occurrence of strong winds usually accompanies with the surge in the offshore environments. In other words, research only on the impact of either wind or wave-induced single loading may underestimate the interaction effect. Hence, the necessity to propose a failure assessment methodology for offshore facilities with combined environmental loads is considerable to guide the safety operation.

Some researchers proceed to survey the dynamic response of offshore facilities from the sight of the survivability in harsh environments. Abdel Raheem [12] evaluated the displacement, axial force, and nonlinear behaviour of the offshore platform under wave-induced loads using Morison's equation and the finite element method. Wang et al. [13] presented the numerical simulation of

hydrodynamic characteristics investigation of a semi-submersible platform with nonsymmetrical pontoons under different wave directions. Zhu and Ou [14] conducted a series of experiments to calculate the maximum horizontal displacement of a semi-submersible platform with a mooring system. Using the weather conditions of the South China Sea, Li et al. [15] discussed the motion performance of the semi-submersible, tension leg platform (TLP), and Truss Spar. These studies mainly focus on either the six-degree maximum motion behaviours (pitch, yaw, sway, surge, heave and roll) or the stress, deformation and acceleration response instead of ascertaining the anticipate operational risk quantitatively. Therefore, this thesis proposes an integrated framework to assess the operational risk quantitatively with combined wind and wave loads.

1.2 Dynamic Risk Assessment

To evaluate the operational risk of the offshore facilities, the risk assessment is the most necessary part. As explained by Crowl and Louvar [16], the goal of the risk assessment is to estimate the occurrence probabilities with the potential consequences for accidents. Many researchers have proposed many related methodologies that are successfully applied in the industrial circle. In general, two main categories are able to represent the previous efforts: (1) Qualitative methods and (2) Quantitative methods. The differences between the two above methods are list as follows.

Method (1) is usually used as a screening process that tends to be applied to a large group of process systems because it provides a relative risk result. In contrast, method (2) is more comprehensive aiming at individual components or

technological processes and first developed by the USNRC (United States Nuclear Regulatory Commission). Either deterministic or probabilistic results calculate the risk for the target components or technological process with a concrete value.

Dynamic Risk Assessment (DRA) can guide the decision-making process for systems due to its nature, the basis of which is the risk analysis approach. The most popular and sophisticated approaches are the Bow-tie (BT) and the Bayesian network (BN). BT consists of two sub approaches which are Fault Tree Analysis (FTA) and Event Tree Analysis (ETA) according to the logic sequence. BT relies on the ability to analyze the basic events which are the failures of the components or operational process to form the intermediate events which further lead to the top event. Then the various combination of the failure of safety barriers eventually causes different accident scenarios. BT is widely applied in many fields [17-21] because of the easily adopted feature and simplicity.

BT has the limitation to express the complex accident causation with traditional logic gates, such as AND & OR gates, the applications of which are not enough to be further expanded. Bayesian network (BN) receives researchers' attention due to the reason that conditional probability tables (CPT) solve the problems. BN is a directed acyclic graphic model, which has the ability to use nodes and arcs to represent variables and relationships among them along with the conditional probability tables [22].

Khakzad et al. [23] illustrated the algorithm of how to map BT with BN with the application of probability updating and probability adapting. BN is capable of depicting the complex logic order of events and incorporating the probability of failures (PoF) at the level of subsystems to the overall system. BN also has the

advantage of performing probability updating and adapting [23-24] because of the unique characteristics for applying Bayes' theorem in nature.

With the advantages, BN is applied by many scholars in different industrial fields, especially in the offshore operation field. Bouejla et al. [25] developed a BN which consisted of environmental limitations, threat characteristics and targets under attack to assess the risks of piracy attacking offshore oil fields. Khakzad et al. [26] used hierarchical Bayesian analysis to estimate the probability of failure for offshore blowouts in the Gulf of Mexico, which can be applied to prevent major accidents. Abimbola et al. [27] analyzed the high safety risk proposed by MPD using BN with the intrinsic characteristics of dependencies modeling and precursor data updating.

Many attempts have been made to apply other methods to improve BN. For example, Guo et al. [24] proposed an innovative copula-based BN model that developed joint non-linear relationships of process variables for decommissioning process risk assessment. Khakzad et al. [28] employed an object-oriented BN risk model considering time dependencies and physical parameters to quantify offshore drilling operation risk.

In this thesis, the BN is applied and served as a robust tool to integrate the probabilities of failure at the level of components' sections calculated by the physical reliability model to the level of components. Then, the failure probability of the systems (offshore facilities) is estimated by incorporating the probabilities of failure of essence structural components based on the units' configuration. The conditional probability tables stand for the mutual influence which reflects the damage caused by the falling debris from the adjacent sections and components.

1.3 Copula-based Dependency Analysis

As mentioned in the previous section, researchers and engineers have applied related standards to calculate environmental loads in order to study the dynamic response or to better design the structural configuration of the offshore facilities. These standards are usually recommended by some authoritative classification societies, such as those used by DNV GL [29] and the American Bureau of Shipping (ABS) [30]. For example, DNV GL standards were used by Suja-Thauvin et al. [31] to compare the results of numerical simulation and the experimental data of the monopile offshore wind turbine. To optimize design the configuration of the 7th generation semi-submersible drilling unit (CSDU), Li et al. [32] calculated hydrodynamic loads with the aid of the ABS rules.

However, it is obvious that the traditional approaches assess the operational safety and risk for offshore facilities without considering the dependency among parameters to calculate the environmental loads. In contrast, the harsh offshore weather conditions may pose a risk to these facilities that are several higher than expected. As a result, the occurrences of catastrophic accidents could be triggered causing great loss and damage to crewmember lives, property, and environment. Therefore, the research should be done to investigate the dependence structure to prevent potential accidents to the greatest extent possible.

When it comes to dependence measurement, the Pearson linear correlation is the most commonly used parameter because of the simple calculation procedure [33]. However, it needs to be clarified that the Pearson linear correlation parameter

follows the assumption of the corresponding elliptical multivariate distribution [34]. It suits for examples like the bivariate normal distribution, which is far from being as realistic as possible. More complex dependence structures call for a more sophisticated approach.

Instead of relying on the linear correlation, copula functions address the limitation to simulate complicated dependencies with the help of rank correlation. *Kendall's tau* and *Spearman's rho* are two typical rank correlation parameters which are a kind of concordance measure. Due to the natural scalar measure of the rank correlation, monotonically transformations of the marginal random distributed variables fail to change the dependencies. In other words, the scale-invariant dependence measures of the rank correlation determine the marginal distribution-free characteristic of the copula functions [35].

The most widely applied copulas are broadly divided into two main categories, which are known as the explicit copulas and the implicit copulas [36]. The implicit copulas are also called elliptical copulas which are derived from multivariate distribution functions without closed-form integral solutions, such as the Gaussian copula and the Student's t-copula. However, the explicit copulas, such as the Clayton copula, the Gumbel copula and the Frank copula which are members of the Archimedian copula family, have simple closed forms that are usually applied to low-dimensional systems [37].

Several available methods have been put forward to estimate the parameters of the copula models. Manner [38] summarized five mature methods of the copula parameter estimation which are known as the exact maximum likelihood (EML) method, inference functions for margins (IFM) method, canonical maximum

likelihood method (CML) and two nonparametric estimation methods. The EML and IFM are two parametric estimation methods while the CML is a semiparametric estimation method.

Copula was first applied by economists to assess the financial risk because of its ability to simulate complex tail dependencies. Manner [38] applied copulas to simulate the exchange rate returns of Latin American currencies against the euro. Melo et al. [39] used copulas to investigate the dependence behaviour of crude oil and gasoline prices aiming to maximize the portfolio return. The copula gradually comes into the application of the system safety and risk analysis with its potential prevailing advantages. Pariyani et al. [40] applied the multivariate normal copula and the Cuadras–Augé copula to study the interdependencies among the failure probabilities of the safety, quality and operability systems. Hashemi et al. [37] developed multivariate loss functions for process facilities operational loss modeling that linked the marginal univariate loss functions with copula functions. In this thesis, dependence functions among parameters to calculate the environmental loads are described by the copulas.

1.4 Research objective of the thesis

The objective of this thesis is to analyze the operational risk of offshore facilities in harsh environments. To be more specific, the research is implemented to fulfill the following academic goals:

- To assess the operational risk of the Semi-submersible Mobile Unit (SMU) quantitatively with combined wind and wave loads in a harsh environment.
- To investigate the influence of the dependence function among real-time

parameters to calculate environmental loads in terms of the impact on the failure probability.

The first objective of this research is the development of the procedure to estimate the anticipated operational risk of the SMU under combined loads. As mentioned before, an operational risk calculation model overcomes the limitation of lacking safety operation envelope reference for decision-makers. This procedure associates related environmental loads calculation model and physical reliability model which transfers the dynamic loads into probabilities of failure (POF). In addition, the Bayesian network (BN) serves as a tool to integrate POF at the level of the SMU.

The second objective of this thesis is the demystification of the effect of dependence structure among real-time observed parameters to calculate the environmental loads, which is a further extension of the first objective. As an obvious fact that environmental parameters such as wind speed and wave heights interact with each other. However, classification societies' standards lack the consideration of the non-linear dependencies. Therefore, in-situ wave and concurrent meteorological observation data available online from the Department of Fisheries and Oceans Canada (DFO) should be employed to simulate the loads and impact on the failure probabilities of the system.

.

1.5 Thesis structure

This thesis is written in the manuscript format. It includes two peer-reviewed journal manuscripts, one of which shown in Chapter 2 is accepted and published on the Ocean Engineering journal and the other one presented in Chapter 3 is

submitted to the Ocean Engineering journal, as well. The outlines of the aforementioned chapters are introduced as follows and shown in Figure 1-1.

Chapter 1 briefly introduces the previous research on the simulations of the dynamic response of the offshore facilities and standards applications based on the classification societies such as those used by DNV GL and the American Bureau of Shipping (ABS). Furthermore, the latest applications of the BN and copula models are covered in this chapter.

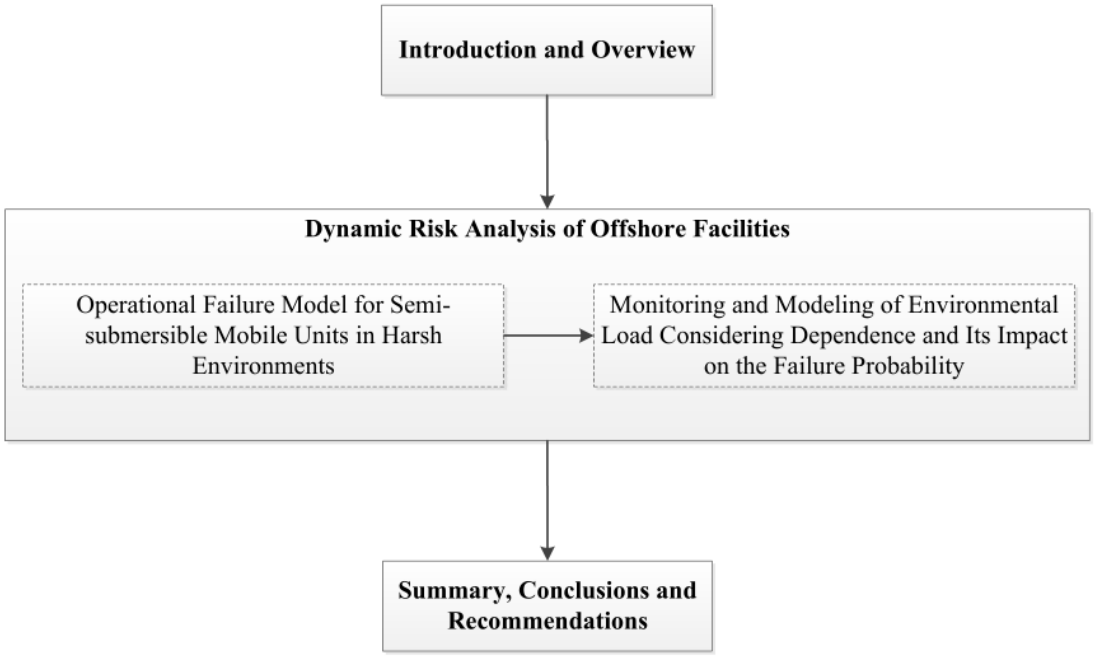

Figure 1-1. Flow diagram of the thesis structure

Chapter 2 includes a manuscript published in the Ocean Engineering journal in 2019. It proposes a methodology which recommends a rigorous procedure to assess the anticipated operational risk of the SMU in harsh environments. With the aid of DNVGL standards and physical reliability model, the probabilities of failure at the level of structural sections are captured, which are further incorporated by the BN. Then a well-known case application – the Ocean Ranger

confirms the effectiveness of the model, which helps to promote safe and reliable offshore development.

Chapter 3 presents a manuscript submitted to the Ocean Engineering journal. A robust copula-based bivariate operational failure assessment model which considers the dependence functions among parameters to calculate the environmental loads is proposed in this study. Wave and concurrent meteorological observation data are accessed from the buoy: Banquereau – 44139 (available online from the Department of Fisheries and Oceans Canada (DFO)). The comparison study of the proposed approach with the traditional approach considering independence validates the robustness of the proposed risk analysis model,

Chapter 5 summarizes the conclusions of the thesis and points several potential research improvements and directions.

1.6 References

[1] Kaiser, M. J., & Yu, Y. (2010). The impact of Hurricanes Gustav and Ike on offshore oil and gas production in the Gulf of Mexico. Applied Energy, 87(1), 284-297.

[2] Cruz, A. M., & Krausmann, E. (2009). Hazardous-materials releases from offshore oil and gas facilities and emergency response following Hurricanes Katrina and Rita. Journal of Loss Prevention in the Process Industries, 22(1), 59-65.

[3] Beven, J. L., Avila, L. A., Blake, E. S., Brown, D. P., Franklin, J. L., Knabb, R.

D., ... & Stewart, S. R. (2007). Annual summary: Atlantic hurricane season of 2005. Monthly Weather Review, 136, 1109-1173.

[4] Cruz, A. M., & Krausmann, E. (2008). Damage to offshore oil and gas facilities following hurricanes Katrina and Rita: An overview. Journal of Loss Prevention in the Process Industries, 21(6), 620-626.

[5] Guan, F., Zhou, C., Wei, S., Wu, W., & Yi, X. (2014). Load-Carrying Capacity Analysis on Derrick of Offshore Module Drilling Rig. Open Petroleum Engineering Journal, 7, 29-40.

[6] Bea, R., Iversen, R., Xu, T., (2001). Wave-in-deck forces on offshore platforms. Journal of offshore mechanics and arctic engineering, 123 (1), 10-21.

[7] Lee, J.-c., Jeong, J.-h., Wilson, P., Lee, S.-s., Lee, T.-k., Lee, J.-H., Shin, S.-c., (2018). A study on multi-objective optimal design of derrick structure: Case study. International Journal of Naval Architecture and Ocean Engineering, 10 (6), 661-669.

[8] Zhu, H., & Ou, J. (2011). Dynamic performance of a semi-submersible platform subject to wind and waves. Journal of Ocean University of China, 10(2), 127-134.

[9] Gonçalves, R. T., Rosetti, G. F., Fujarra, A. L., & Oliveira, A. C. (2013). Experimental study on vortex-induced motions of a semi-submersible platform with four square columns, Part II: Effects of surface waves, external damping and draft condition. Ocean engineering, 62, 10-24.

[10] Liu, H., Chen, G., Lyu, T., Lin, H., Zhu, B., & Huang, A. (2016). Wind-induced response of large offshore oil platform. Petroleum Exploration

and Development, 43(4), 708-716.

[11] Lee, S. K., Yu, K., & Huang, S. C. (2014). CFD study of air-gap and wave impact load on semisubmersible under hurricane conditions. Paper presented at the ASME 2014 33rd International Conference on Ocean, Offshore and Arctic Engineering. San Francisco, USA

[12] Abdel Raheem, S. E. (2016). Nonlinear behaviour of steel fixed offshore platform under environmental loads. Ships and Offshore Structures, 11(1), 1-15.

[13] Wang, S., Cao, Y., Fu, Q., & Li, H. (2015). Hydrodynamic performance of a novel semi-submersible platform with nonsymmetrical pontoons. Ocean Engineering, 110, 106-115.

[14] Zhu, H., & Ou, J. (2011). Dynamic performance of a semi-submersible platform subject to wind and waves. Journal of Ocean University of China, 10(2), 127-134.

[15] Li, B., Liu, K., Yan, G., & Ou, J. (2011). Hydrodynamic comparison of a semi-submersible, TLP, and Spar: Numerical study in the South China Sea environment. Journal of Marine Science and Application, 10(3), 306.

[16] Crowl, D. A., & Louvar, J. F. (2011). Chemical Process Safety-Fundamentals with Applications. Process Safety Progress, 30(4), 408-409.

[17] Ferdous, R., Khan, F., Sadiq, R., Amyotte, P., & Veitch, B. (2013). Analyzing system safety and risks under uncertainty using a bow-tie diagram: An innovative approach. Process Safety and Environmental Protection, 91(1-2), 1-18.

[18] Lu, L., Liang, W., Zhang, L., Zhang, H., Lu, Z., Shan, J., (2015). A comprehensive risk evaluation method for natural gas pipelines by combining a risk matrix with a bow-tie model. Journal of Natural Gas Science and Engineering 25, 124-133.

[19] Abimbola, M., Khan, F., & Khakzad, N. (2014). Dynamic safety risk analysis of offshore drilling. Journal of Loss Prevention in the Process Industries, 30, 74-85.

[20] Khakzad, N., Khan, F., & Amyotte, P. (2012). Dynamic risk analysis using bow-tie approach. Reliability Engineering & System Safety, 104, 36-44.

[21] Yuan, Z., Khakzad, N., Khan, F., Amyotte, P., & Reniers, G. (2013). Risk-based design of safety measures to prevent and mitigate dust explosion hazards. Industrial & engineering chemistry research, 52(50), 18095-18108.

[22] Yeo, C., Bhandari, J., Abbassi, R., Garaniya, V., Chai, S., Shomali, B., (2016). Dynamic risk analysis of offloading process in floating liquefied natural gas (FLNG) platform using Bayesian Network. Journal of Loss Prevention in the Process Industries 41, 259-269.

[23] Khakzad, N., Khan, F., & Amyotte, P. (2013). Dynamic safety analysis of process systems by mapping bow-tie into Bayesian network. Process Safety and Environmental Protection, 91(1-2), 46-53

[24] Guo, C., Khan, F., & Imtiaz, S. (2019). Copula-based Bayesian Network Model for Process System Risk Assessment. Process Safety and Environmental Protection.

[25]Bouejla, A., Chaze, X., Guarnieri, F., & Napoli, A. (2014). A Bayesian network to manage risks of maritime piracy against offshore oil fields. Safety science, 68, 222-230.

[26] Khakzad, N., Khakzad, S., & Khan, F. (2014). Probabilistic risk assessment of major accidents: application to offshore blowouts in the Gulf of Mexico. Natural Hazards, 74(3), 1759-1771.

[27] Abimbola, M., Khan, F., Khakzad, N., & Butt, S. (2015). Safety and risk analysis of managed pressure drilling operation using Bayesian network. Safety science, 76, 133-144.

[28] Khakzad, N., Khan, F., & Amyotte, P. (2013). Quantitative risk analysis of offshore drilling operations: A Bayesian approach. Safety science, 57, 108-117.

[29] DNVGL-RP-C205, Enviromental conditions and enviromental loads. August 2017. DNV GL

[30] American Bureau of Shipping (ABS), Rules for building and Classing Mobile Offshore Drilling Units. 2019

[31] Suja-Thauvin, L., Krokstad, J. R., & Bachynski, E. E. (2018). Critical assessment of non-linear hydrodynamic load models for a fully flexible monopile offshore wind turbine. Ocean Engineering, 164, 87-104.

[32] Li, D. J., Fu, Q., Du, Z. F., Xiao, Y., Han, R. G., & Sun, H. H. (2018). Structural Configuration Selection and Optimization of 7th Generation Semi-Submersible Drilling Unit. Paper presented at the ASME 2018 37th International Conference on Ocean, Offshore and Arctic Engineering. Madrid, Spain.

[33] Klaus, M. (2013) Multivariate Dependence Modeling using Copulas. Master Thesis. Charles University in Prague.

[34] Hashemi, S. J., Ahmed, S., & Khan, F. I. (2015). Correlation and dependency in multivariate process risk assessment. Paper Presented at the IFAC SAFEPROCESS 2015: 9th IFAC Symposium on Fault Detection, Supervision and Safety for Technical Processes, Paris, France.

[35] Nelsen, R.b., (2006). An introduction to Copulas, second ed. Springer, New York, NY.

[36] Hashemi, S.J., (2016). Dynamic multivariate loss and risk assessment of process facilities. Doctoral (PhD) thesis, Memorial University of Newfoundland.

[37] Hashemi, S. J., Ahmed, S., & Khan, F. (2015). Operational loss modelling for process facilities using multivariate loss functions. Chemical Engineering Research and Design, 104, 333-345.

[38] Manner, H. (2007). Estimation and model selection of copulas with an application to exchange rates. (METEOR Research Memorandum; No. 056). Maastricht: METEOR, Maastricht University School of Business and Economics

[39] Melo, R., Accioly, S., & Aiube, F. A. L. (2008). Analysis of crude oil and gasoline prices through copulas. Cadernos do IME-Série Estatística, 24(1), 15.

[40] Pariyani, A., Seider, W. D., Oktem, U. G., & Soroush, M. (2012). Dynamic risk analysis using alarm databases to improve process safety and product quality: Part II—Bayesian analysis. AIChE Journal, 58(3), 826-841.

Chapter 2. Operational Failure Model for Semi-submersible Mobile Units in Harsh Environments[1]

Jinjie Fu and Faisal Khan*

Centre for Risk, Integrity and Safety Engineering (C-RISE),

Faculty of Engineering and Applied Science,

Memorial University of Newfoundland, St. John's, NL, A1B 3X5, Canada

Abstract

The Semi-submersible Mobile Unit (SMU) plays a vital role in the development of offshore oil and gas fields. Extreme weather conditions such as high winds, waves, and icy conditions impose an extraordinary load on the platform. This paper presents a detailed operational failure model considering the wind and wave combined loading of extreme weather conditions. The model is developed in a probabilistic framework using the Bayesian network (BN) to assess the operational risk quantitatively. The BN represents conditional dependencies of the weather effects and the operational characteristics of the SMU. The proposed model is tested and validated using a well-known accident - the Ocean Ranger. The model predicts a very high probability of operational failure (capsizing) in the prevailing weather conditions, which is confirmed by the fateful event on Feb 15, 1982. The proposed model is a useful and reliable tool to develop and monitor the

[1] Fu, J., & Khan, F. (2019). Operational failure model for semi-submersible mobile units in harsh environments. Ocean Engineering, 191, 106332.

operational failure envelope of the SMU in given environmental conditions. This work helps to promote safe and reliable offshore development.

Keywords: Operational failure; Bayesian network; Physical reliability model; Semi-submersible unit; Wind and wave load; Offshore failure model

2.1 Introduction

With the acceleration of urbanization, land based oil exploitation alone cannot meet people's growing demand for energy. Attention has therefore shifted to offshore reservoirs, which contain tremendous oil and gas resources. However, due to the complex and changeable marine environment, offshore drilling accidents have occurred frequently in the last few decades. Through the analysis of public records and reports, Ismail et al. (2014) stated that 15.1% of offshore drilling accidents are caused by storms and hurricanes, second only to blowouts over the last 56 years.

Previous research attempted to simulate the single environmental impact load on the SMU. Ma et al. (2017b) developed a numerical simulation model to capture the dynamic stress response of the derrick under random wind loads. Lee et al. (2018) studied derrick performance, considering gravity and wind pressure. Instead of taking the SMU as a whole system, only one or several structural components have been analyzed. Note that all the elements working as a harmonious integration interact with the complicated marine environment. Liu et al. (2018) addressed performance-based analysis for the offshore jacket platform subject to wind loads. Banks and Abdussamie (2017) developed wave and semi-submersible interaction experiments using a piston-type wavemaker. However, these models only analyzed the influence of a specific load with either wind or wave-induced loading through numerical simulation, model experiments, or field tests. Gomathinayagam et al. (2000) identified that wind load only accounts for 20% - 25% of total loads in cyclonic winds. Especially during extreme weather

conditions, any components of the offshore structure may fail subject to wind and wave combined impacts which potentially trigger a series of chain reactions. Therefore, it is crucial to establish a damage assessment framework for the whole SMU system which combines the predominant environmental loads, wind and wave loads, simultaneously.

Research has been conducted to investigate the survivability of offshore platform structure from external loading. Ma et al. (2017a) applied ANSYS and AQWA to estimate structure and motion responses subjected to environmental loads. Ma et al. (2019) put forward an Improved Mixture Simulation (IMS) method aiming to describe stress responses and structural displacement of a semi-submersible offshore platform. 3-D radiation and diffraction theory are employed to determine the frequence and time response of a semi-submersible platform for the 100-year return period of environmental loads (Ghafari and Dardel, 2018). Yu et al. (2018) conducted hydrodynamic behaviour studies of TLP applying the JOHNSWAP wave type. The aforementioned evaluation indicators pay more attention to either external hydrodynamic performance or internal structure dynamic analysis rather than assessing the operational risk quantitatively. Under the practical circumstance, the operators want to ascertain the anticipate risk in the harsh environments to guide the further decision. Consequently, how to evaluate the risk posed by rogue waves and violent winds quantitatively appears to be particularly important.

When it comes to employing risk analysis, quantitative risk assessment (QRA) is a widely used effective technique. Especially in offshore operational fields

(Leimeister and Kolios, 2018) the Bayesian network (BN) is recommended for risk assessment. As a graphic model, it uses nodes and arcs to represent variables and relationships among them along with the conditional probability tables (CPTs). The conditional dependencies are determined by either direct data or subjective expert systems to reduce uncertainty(Yeo et al., 2016). Abaei et al. (2018b) applied the BN to manage the risk arising from the storm of Floating Storage Unit (FSU) based on the hydrodynamic accident load model. Barua et al. (2016) mapped a dynamic fault tree into the Bayesian network to perform a dynamic operational risk assessment with time-dependent characteristics. Song et al. (2016) employed a BN model to investigate occupational risks for offshore operations in harsh environments. Abaei et al. (2018a) integrated hydrodynamic analysis and failure modeling using BN to assess the reliability of marine floating structures. As a result, it can be concluded that BN is capable of estimating the overall operational probability of failure of an offshore structure based on conditional dependencies and subsystems' failure probabilities in harsh environments.

Accordingly, this work aims to propose a robust and reliable operational failure model with the application of the BN for an SMU considering wave and wind combined loads in a harsh environment. To begin with, environmental loads are calculated with the help of wind load response modeling (DNVGL-RP-C205, 2017), the Morison model (DNVGL-RP-C205, 2017) and the ultimate limit states method (DNVGL-RP-C103, 2015). Furthermore, structural components' probabilities of failure are gathered thanks to different physical reliability models and joint probability functions which combine the dynamic probabilistic response

to wind and wave loads. With the application of BN, the present study considers the weather on site and the unit configuration to estimate the overall probability of failure of an SMU, which provides an anticipated operational safety reference value for decision making. This paper is organized as follows: Section 2.2 develops a methodology for operational failure modeling along with a simple case example. The applicability is demonstrated with a case study in Section 2.3. Section 2.4 briefly explains the impact of the operational state and the combined loads, and Section 2.5 concludes the study.

2.2 Methodology to Develop the Operational Failure Model

The proposed methodology to develop the operational failure model takes operational state and ultimate load-bearing capacity into consideration. Then a BN is developed to assess the specific probability of failure under a certain set of circumstances. To better illustrate the methodology, Figure 3-1 explains the framework of operational failure modeling of an SMU. In addition, a simple case example is shown step by step.

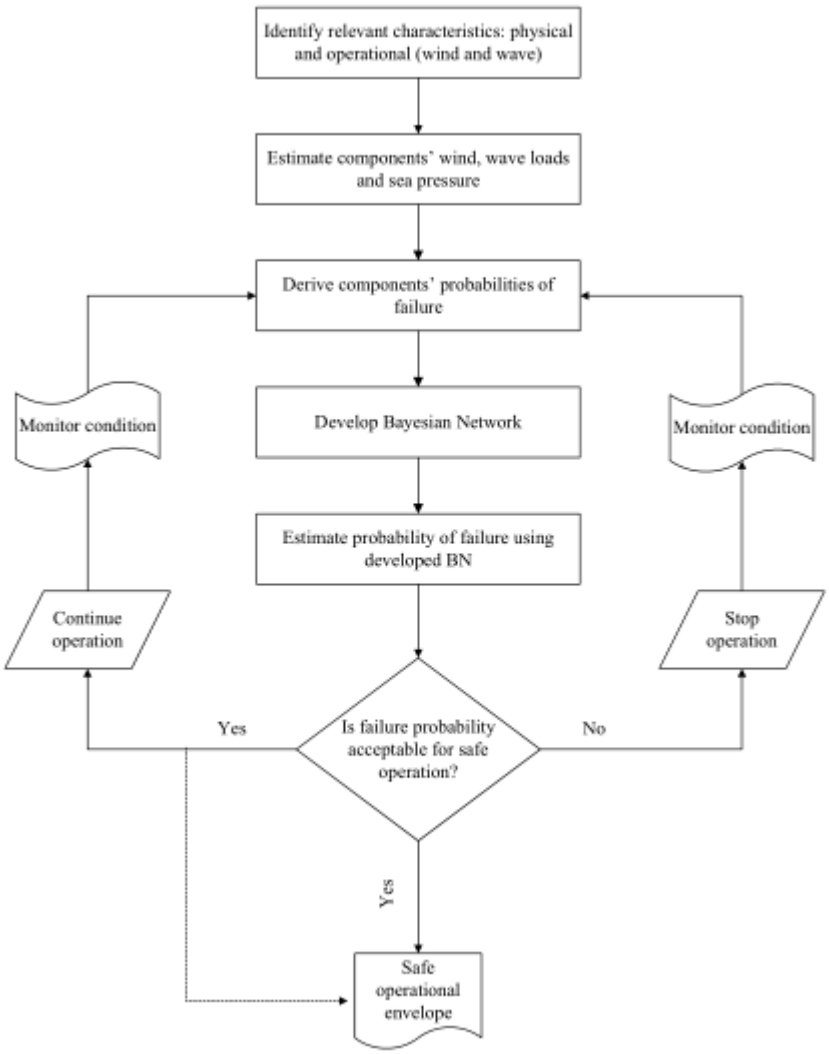

Figure 2-1. Framework of operational failure modeling

2.2.1 **Identify relevant characteristics: physical and environmental**

The first step of the methodology is to identify the physical characteristics, which include the fundamental configuration, operational state, and ultimate environmental conditions. Subsequently, weather conditions on the scene should be clarified through related weather forecasts. A simplified case is used to demonstrate the operational risk assessment model for the SMU. Table 2-1 shows

the geometric dimensions of the example SMU. For the sake of simplicity, the aim is to assess the operational probability of failure under the harsh weather conditions of 80 knots wind speed and 70 ft wave height. Holmes (2015) developed the power law profile to describe the wind speed above the ground. The profile used a reference mean wind speed for 10 minutes at 10 m height above ground.

$$\bar{U}(z) = \bar{U}(H)(\frac{z}{H})^{z_0} \quad (2.1)$$

where z is the height, $\bar{U}$(H) is the reference mean wind speed for 10 minutes, H is the reference height equal to 10m and z_0 is the terrain roughness parameter.

Table 2-1 Main dimensions of the example SMU

Component	Dimension	Component	Dimension
Length of pontoons	200 ft	Upper deck	150 ft
Height of pontoons	20 ft	Lower deck	120 ft
Width of pontoons	20 ft	Operational draft	80 ft
Diameter of columns	30 ft	Height of derrick	160 ft
Height of columns	100 ft	Affordable wind speed	100 knots
Number of columns	4	Affordable wave height	100 ft

Wave fluid particle speed and acceleration are derived from the derivative of the wave velocity potential concerning displacement and then time, respectively. The formulae involved for fluid particle velocity and acceleration of the corresponding second-order Stokes wave theory are provided in DNVGL-RP-C205 (2017).

2.2.2 **Sections' division and estimate components' environmental loads**

According to the offshore structure design standard (DNVGL-OS-C201 2017; DNVGL-OS-C101 2019; DNVGL-OS-C201, 2017), it is essential to take environmental loads, wind and hydrodynamic loads induced by waves into consideration for mobile offshore units operating under harsh environmental conditions.

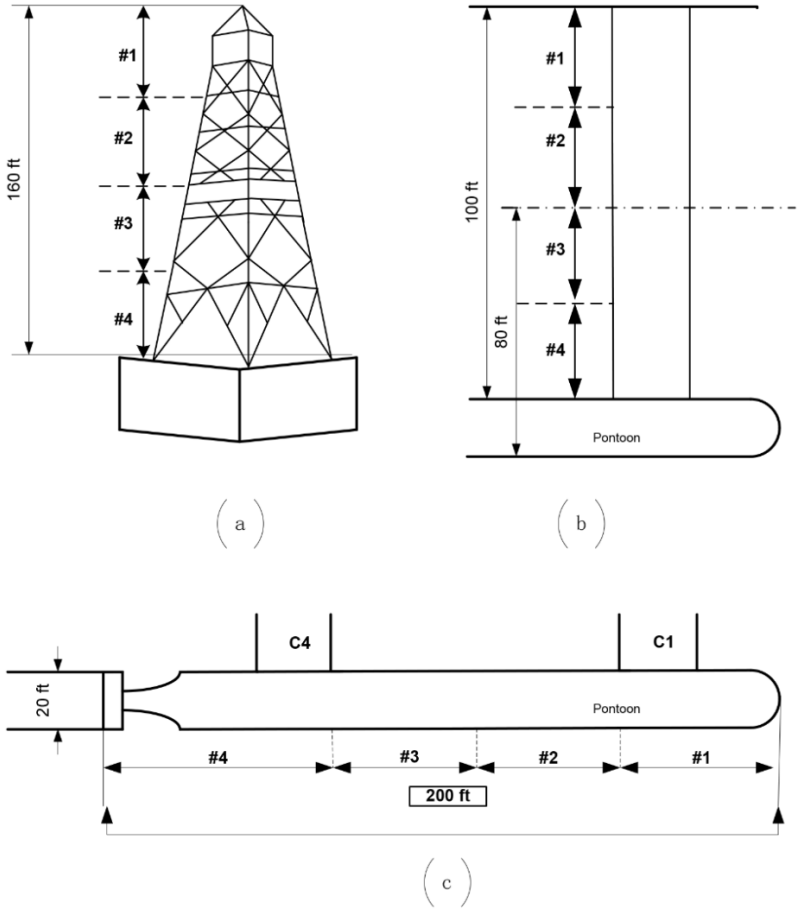

Figure 2-2. Schematic diagram for derrick (a), column (b) and pontoon (c) of the example SMU with generated sections

The SMU is a widely deployed engineering equipment for offshore deep-water oil

and gas development, which mainly consists of a derrick, deck, columns, and pontoons. In order to better assess the response of structural components' probabilities of failure in detail, the main components of the unit, consisting of the derrick, pontoons, and columns, are divided into four generated sections (from section #1 to #4) as indicated in Figure 2-2. Every section includes many nodes which are statistically finite. To be noticed, these sections are also developed to form root nodes of the BN. As a result, wind and wave characteristics are determined through a wind speed profile and second-order Stokes wave theory. Accordingly, Table 2-2 presents wind, wave load, and sea pressure, which are calculated for sections through wind load response modeling, the Morison model and the ultimate limit states method.

Table 2-2 Load calculation models

Load	Model
Wind load	Wind load response modeling (DNVGL-RP-C205, 2017)
Wave load	Morison model (DNVGL-RP-C205, 2017)
Sea pressure	Ultimate limit states method (DNVGL-RP-C103, 2015)

Although the vertical wave loads sometimes exceed horizontal wave loads for the SMU, buoyancy force and gravitational force partially counteract the effects of the waves' force. Additionally, the deck is usually designed as grated and open (non-plated) to reduce all kinds of contamination in the deck area, and to avoid slip/fall accidents. Bea et al. (2001) insisted that vertical force is negligible compared to horizontal force on open, grated decks. Technically, the crux of the

proposed methodology is to capture the probability of failure by incorporating the ultimate load and operational load, regardless of the direction, into the physical reliability model. Hence, only the horizontal wave load and sea pressure are discussed in this paper. The permissible loads and actual loads on the basis of real weather on the scene are presented in Table 2-3.

2.2.3 **Derive components' probabilities of failure under combined loads**

The physical reliability model assumed that reliability is independent of the time parameter (Khakzad et al., 2012). In this model, the relationship between stress and strength is analyzed through a given distribution of the variables. The probability of failure can be quantified by integrating the stress or strength distribution. Intuitively, the loads are randomly distributed because of random weather conditions in nature, as reflected in part (a) of Figure 2-3. However, every section presented in Figure 2-2 includes many nodes, which are statistically finite, as mentioned. Every black line in part (a) of Figure 2-3 represents various nodes' resistance to loads, which involve their specific responses owing to stress concentration, unit configuration, and so on, to different loads. For a particular node, there exists a unique probabilistic response for dynamic external loads. Then, it is assumed that the dynamic probabilistic response of all nodes in an individual section follows lognormal distribution, for mathematical convenience, with location parameter t_{med} and shape parameter as shown in part (b) in Figure 2-3. The x-coordinate represents the corresponding maximum bearable weather response index such as wind speed or wave height, for all nodes in a certain

section, instead of the physical properties of materials.

$$P(R < L) = \int_0^L f_r(r)\, dr = \Phi(\frac{1}{s} ln \frac{L}{t_{med}}) \quad (2.2)$$

The next step is to determine the shape parameter and location parameter in *Equation (2.2)*. It is worth mentioning that both parameters can be related to mean μ and standard deviation σ through mathematical transformation. A reasonable coefficient of variation (COV) helps to solve them. In the work of Cheng and Yeung (2002), there is nearly 99% certainty that the COV is between 0.05 and 0.20 based on the available wind speed statistical data in 143 weather stations in the United States. Because the marine environment of the SMU is relatively harsh, the COV should be adjusted appropriately to between 0.01 and 0.5. Generally speaking, COV stands for the degree of data concentration and dispersion as shown in Figure 2-4. Compared to the red case, the blue case has a higher COV, which is quite more even and scattered. With the environmental loads producing small variations, the resistance response of the blue case tends to change dramatically due to stronger sensitivity generated by a greater COV. In an interview (Zhang, 2017), Robert Bea, a professor emeritus in civil engineering at the University of California, Berkeley said "The pressures generated in those wave crests can exceed several thousand pounds per square inch,". He argues that "Offshore platforms can generally deal with wind and rainfall okay, but cresting waves will do real damage." Therefore, it is assumed that COV is 0.074 for every section's statistically distributed wind resistance response and 0.1 for statistically distributed wave resistance response for the example SMU.

DNVGL-OS-C101 (2019) suggested that the probability of exceedance for wind and wave induced loads should be no more than 10^{-2} under the maximum design

loads. Once the ultimate load-bearing capacity for each section (loads produced by 100 knots wind speed and 100 ft wave height in the example, respectively) is calculated with load calculation models, L and P are substituted into Equation (2.2) with above loads separately (the first step is to obtain the probability of failure under single load impact) and 10^{-2}. By combinations of simultaneous COV equations, shape and location parameters can be solved to determine the probability of failure under any weather conditions on the scene for non-specific sections against a single load.

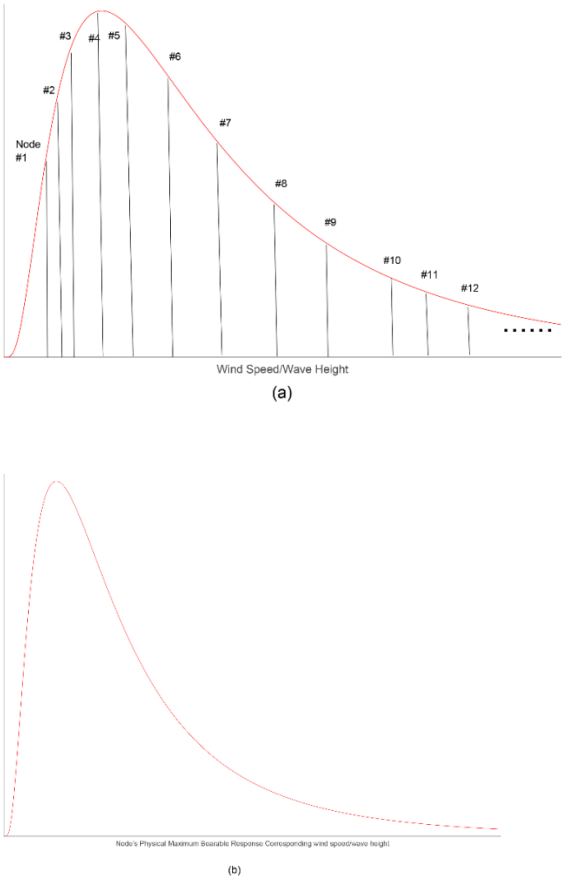

Figure 2-3. (a) Random weather conditions and nodes' response; (b) Node's physical maximum bearable corresponding wind speed/wave height

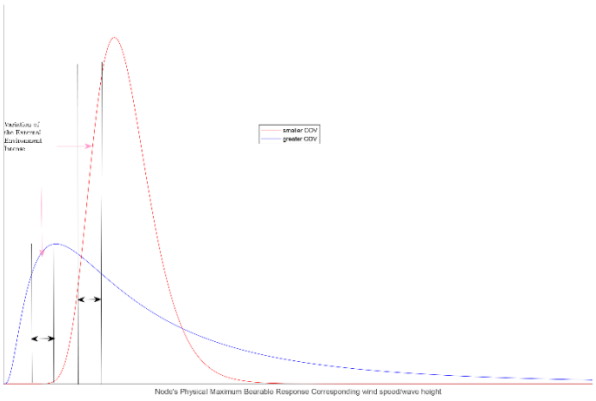

Figure 2-4. Node's physical maximum bearable response corresponding Wind speed/wave height

It is known that the SMU has to deal with multivariate site-specific environmental loads in a harsh environment. For example, wind and wave induced loads affect deck and columns above the draft. Additionally, pontoons and columns below the draft suffer the damage of sea pressure and wave induced loads. In spite of the fact that the probabilistic response for a non-specific section against a single load is solved, sections' different probabilistic responses regarding the different loads need to be combined. In this paper, the sections' response for wind and wave loads are treated differently rather than using simple mathematical addition. As a consequence, a joint probability distribution can be applied to assess the components' probability of failure.

Joint probability functions (Forbes et al., 2011) are known as multivariate distributions, which can describe the distribution of multiple random variances concerning regions of N-dimensional space. Moreover, the probability of a set of

random variables can be obtained through marginalization. A bivariate lognormal distribution is adapted, owing to the fact that not only are there positive values for loads without a clear increasing tendency, but also because the marginal probability distribution follows a lognormal distribution. The probability density function (PDF) of joint and marginal distributions of random variables X and Y is:

$$f(x,y) = \frac{1}{2\pi\sigma_x\sigma_y xy\sqrt{1-\rho^2}} \exp\left\{-\frac{1}{2(1-\rho^2)}\left[\left(\frac{lnx-\mu_x}{\sigma_x}\right)^2 - 2\rho\left(\frac{lnx-\mu_x}{\sigma_x}\right)\left(\frac{lny-\mu_y}{\sigma_y}\right) + \left(\frac{lny-\mu_y}{\sigma_y}\right)^2\right]\right\}$$

$$(x > 0, y > 0, -1 < \rho < 1) \quad (2.3)$$

$$f(x) = \frac{1}{\sqrt{2\pi}\sigma_x x} exp\left(-\frac{1}{2\sigma_x^2}(ln\frac{x}{e^{\mu_x}})^2\right), (x > 0) \quad (2.4)$$

$$f(y) = \frac{1}{\sqrt{2\pi}\sigma_y y} exp(-\frac{1}{2\sigma_x^2}(ln\frac{y}{e^{\mu_y}})^2), (y > 0) \quad (2.5)$$

where ρ is the correlation coefficient, σ_x , σ_y are the standard deviation and μ_x , μ_y are the mean of $\ln X$, $\ln Y$.

To conclude, operationally safe wind and wave loads can be calculated using the design with affordable wind speed and wave height as provided in the SMU safe operation manual, respectively. Then, the annual probability of exceedance is 10^{-2} for the operational safety wind and wave loads, as stipulated by DNVGL-OS-C101 (2019). In addition, marginal probability distribution parameters for every section under a single designed and manufactured maximum load response are calculated combining the assumed simultaneous COV equations. Ultimately, the joint bivariate lognormal distribution is applied to determine the probability of failure for every analytical section under combined loads (X = wind loads and Y = wave loads at sections level). Parameters of the joint bivariate lognormal distribution are from the marginal distributions which are the components'

response to a single load. In this paper, it is assumed that wind load and wave load are independent of each other. Consequently, the correlation coefficient ρ in the joint probability functions equals 0. Under these conditions, the probabilities of failure at components' levels under combined wind and wave induced loading are completed.

During the monitor period in operation, the maximum wind speed and wave height can be observed which are used to gain real time environmental load. Then the loads are substituted into the solved bivariate log-normal distribution to assess the real time operational risk. Table 2-3 summarizes the probabilities of failure for each section of the principal components. Next step is to estimate the overall probability of failure with the aid of the BN.

2.2.4 **Estimate the overall probability of failure using the BN**

A BN is a directed acyclic graphical model (Weber et al., 2012), which is composed of random variables that represent root causes, arcs that clarify dependencies between parent nodes and child nodes, and the conditional probability that quantifies forward predictive inference.

$$P(A) = \sum_{i=1}^{n} P(A|B_i)P(B_i) \qquad (2.6)$$

where $P(A|B_i)$ is conditional probability and $P(B_i)$ is the probability of the i^{th} variable.

Conditional probability tables (CPT) of BNs are achieved according to the weights of events, which come from the survey with prior probabilities of primary events or subjective belief. The weight of an event refers to the likelihood of

occurrence of its upper events, given the event's occurrence. In this paper, subjective opinions satisfy the primary purpose of assessing the probabilities of operational failure in a harsh environment. The sixth generation of the deep water SMU mainly consists of a derrick, deck, columns, and pontoons. The deck houses all drilling machinery, including the derrick, material storage, and living facilities. Columns are located between the deck and pontoons, supporting the unit with four to eight vertical cylinders. Pontoons composed of oil tanks, ballast water tanks and drill water tanks provide flotation to the system. In the demonstration example, only corner columns are considered. Figure 2-5 illustrates the general BN assessing the probability of failure of an example SMU. The root nodes are from the sections of each structural component. DS 1 - 4 represent sections #1 to #4 of the derrick. Similarly, CS 1 – 4 and PS 1 - 4 represent sections #1 to #4 of the corner columns and pontoons, as illustrated in Figure 2-2.

In order to distinguish the damage caused by the section itself (response to environmental loads) and the adjacent section, the suffix 'S' is applied. For example, DS3 indicates the damage caused by environmental loads to section #3 of the derrick directly and DS3S expresses the damage caused by both environmental loads directly and collateral debris from section #2 of the derrick. Because of the unit configuration, it is assumed that only two adjacent sections interact with the debris trajectory. In short, the greater the height of the section, the greater the mutual influence factor is, since the uppermost section has the strongest potential of both kinetic and gravitational failure. In this paper, failure of any component (derrick, deck, column and pontoon) triggers the damage to the overall platform. Finally, BN combines all the structural components to estimate

the overall probability of failure (PoF) under the weather on the scene to create a general assessing framework. The results of the operational probabilities of failure for components and the platform are presented in Table 2-3.

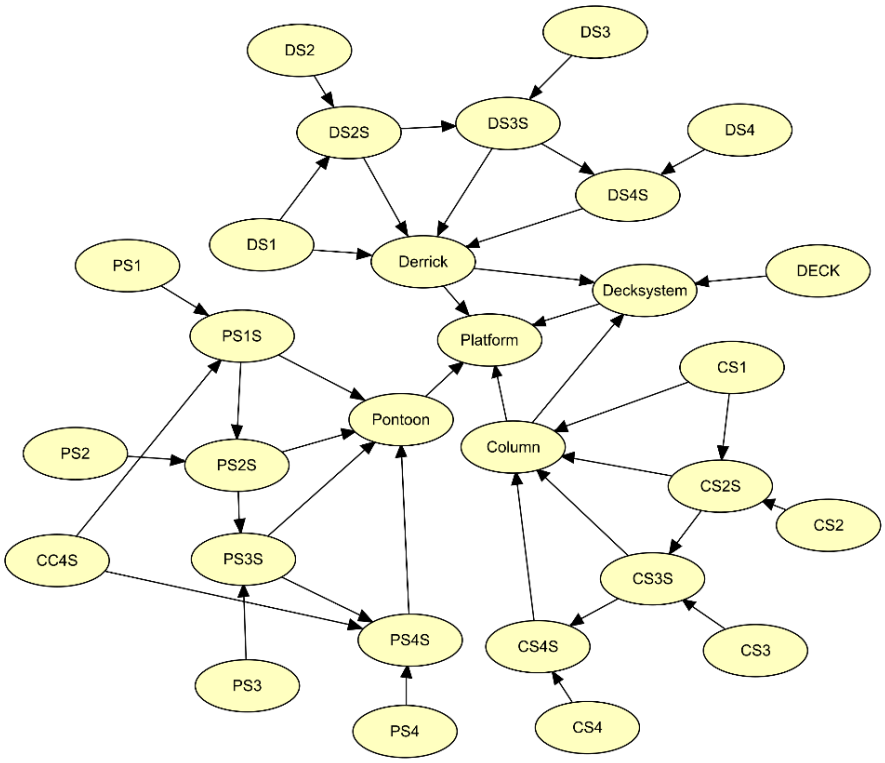

Figure 2-5. Generic BN of operational failure modeling

Table 2-3 Nodes illustration in generic BN

	Permissible Load			Actual Load			PoF
Component	Wind	Wave	Sea pressure	Wind	Wave	Sea pressure	
	10^3 Pa	10^4 Pa	10^5 Pa	10^3 Pa	10^4 Pa	10^5 Pa	
Derrick	-	-	-	-	-	-	4.00×10^{-4}
Section #1	3.42	-	-	2.19	-	-	1.07×10^{-4}

Section #2	3.25	-	-	2.08	-	-	1.04×10^{-4}
Section #3	3.04	-	-	1.95	-	-	1.17×10^{-4}
Section #4	2.79	-	-	1.78	-	-	8.79×10^{-5}
Deck	2.47	7.60	-	1.58	3.23	-	1.64×10^{-5}
Columns	-	-	-	-	-	-	7.07×10^{-5}
Section #1	2.14	3.43	-	1.37	2.41	-	1.23×10^{-5}
Section #2	1.57	3.05	-	1.00	2.17	-	1.15×10^{-5}
Section #3	-	2.65	4.16	-	1.90	3.82	2.91×10^{-8}
Section #4	-	2.25	5.13	-	1.62	4.8	4.69×10^{-5}
Pontoons	-	-	-	-	-	-	7.00×10^{-5}
Section #1	-	1.52	5.95	-	1.05	5.61	1.60×10^{-5}
Section #2	-	1.52	5.95	-	1.05	5.61	1.60×10^{-5}
Section #3	-	1.52	5.95	-	1.05	5.61	1.60×10^{-5}
Section #4	-	1.52	5.95	-	1.05	5.61	1.60×10^{-5}
SMU	-	-	-	-	-	-	6.00×10^{-4}

The simulation results in Table 2-3 show that the platform will bear a tolerable probability of failure if it operates under 80 knots of wind and a 70 ft wave height simultaneously. Generally, in accordance with DNVGL-OS-C101 (2019), the operational failure envelope of in situ operational probability of failure can be defined as $[10^{-2}, 1]$. The explanation for the operational failure envelope is that the higher the failure probability of the system, the greater the destructive potential. Once the result of operational failure modeling based on weather data on the scene is calculated, further recommendations are suggested to avoid catastrophic disaster. If the estimated probability of failure falls in the operational failure envelope, it is recommended to terminate the operation and drag the SMU back to

the harbour to reduce risk. In contrast, it is allowed to continue operating if the proper procedure is followed and real-time conditions are monitored in case of rapidly changing weather conditions. As an anticipated risk estimation model, the proposed operational failure model is capable of capturing real-time weather data on the scene and the current operational state to provide a safety operational perspective.

2.3 Testing of the model - the Ocean Ranger Disaster

To verify the proposed methodology, a case study was conducted. The aim of the case study was to model the prevailing conditions during the Ocean Ranger oil rig disaster. The accident occurred off the coast of Newfoundland on Feb 15, 1982. Heising and Grenzebach (1989) earlier studied this accident using a fault tree with a beta factor to assess the capsize probability of the Ocean Ranger. Several core components, including pumps, valves, and onboard liquids, were utilized to analyze the failure probability using common cause failure. According to the Marine Casualty Report - Mobile Offshore Drilling Unit (MODU) Ocean Ranger (US Coast Guard, 1983), rogue waves which were still in the acceptable height range attacked the Ocean Ranger. Due to the design flaw, the ballast control room with the open deadlight was located close to the drilling draft water line. As a result, the rig capsized and sank in the Grand Banks area, 267 kilometers east of St. John's, Newfoundland (US Coast Guard, 1983).

2.3.1 **Identify SMU's physical characteristics and weather condition**

To begin, Table 2-4 illustrates the geometric scale parameters of the Ocean Ranger. According to the final report by the US Coast Guard (1983), the Ocean Ranger was able to withstand 100-knot winds and 110-ft waves at the same time. Subsequently, the wind speed predictive development model is the basis of the entire risk assessment process, owing to the fact that both the wind's inflicted destruction potential and wind-induced wave damage are dominated by wind speed. Thus, a simple empirical database derived hurricane wind model is adapted for predicting the maximum wind of tropical cyclones (Kaplan and DeMaria, 1995).

Table 2-4 Physical characteristics of the Ocean Ranger (US Coast Guard, 1983)

Component	Dimension	Component	Dimension
Length of pontoons	398.6 ft	Drilling draft	80 ft
Height of pontoons	24 ft	Height of derrick	185.4 ft
Width of pontoons	62 ft	Diameter of corner columns	36 ft
Upper deck	151.6 ft	Diameter of middle columns	25 ft
Lower deck	134 ft	Height of ballast control room	108 ft
Height of columns	110 ft	Affordable wind speed	100 knots
Number of columns	8	Affordable wave height	110 ft

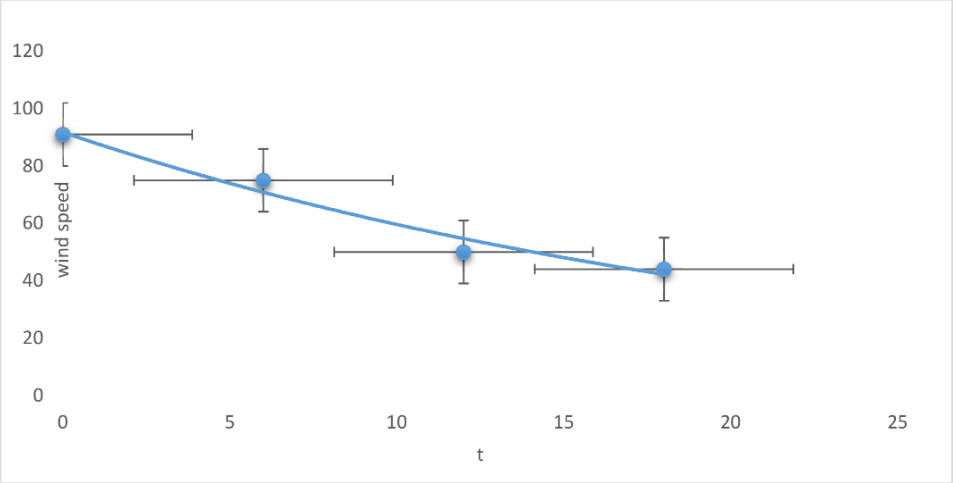

Figure 2-6. Wind speed decay matching tendency model dependent on weather data on the scene (US Coast Guard, 1983)

The empirical decay model was derived based on landfall hurricanes, which makes the application of the landfall reduction factor, R, and the effect of the distance inland-reduction term, C, superfluous when dealing with an offshore hurricane. Therefore, the modified hurricane wind speed decay model utilizes the weather report data (US Coast Guard, 1983) of 14/15 February 1982 when the Ocean Ranger sank, as below：

$$V(t) = V_b + (V_0 - V_b)e^{-\alpha t} = 26.7 + (90 - 26.7)e^{-0.043t} \quad (2.7)$$

where V_b is background wind speed, V_0 is maximum sustained 1-min surface wind speed and α is the decay constant (h^{-1}).

Figure 2-6 indicates that the maximum sustained 1-min wind speed is 90-knot, which is below the ultimate wind speed for the Ocean Ranger. The testimony and radio conversations (US Coast Guard, 1983) indicated that rogue waves up to 65 ft attacked the Ocean Ranger, which destroyed the unprotected portlight of the

ballast control room.

2.3.2 **Divide components' sections and calculate corresponding environmental loads**

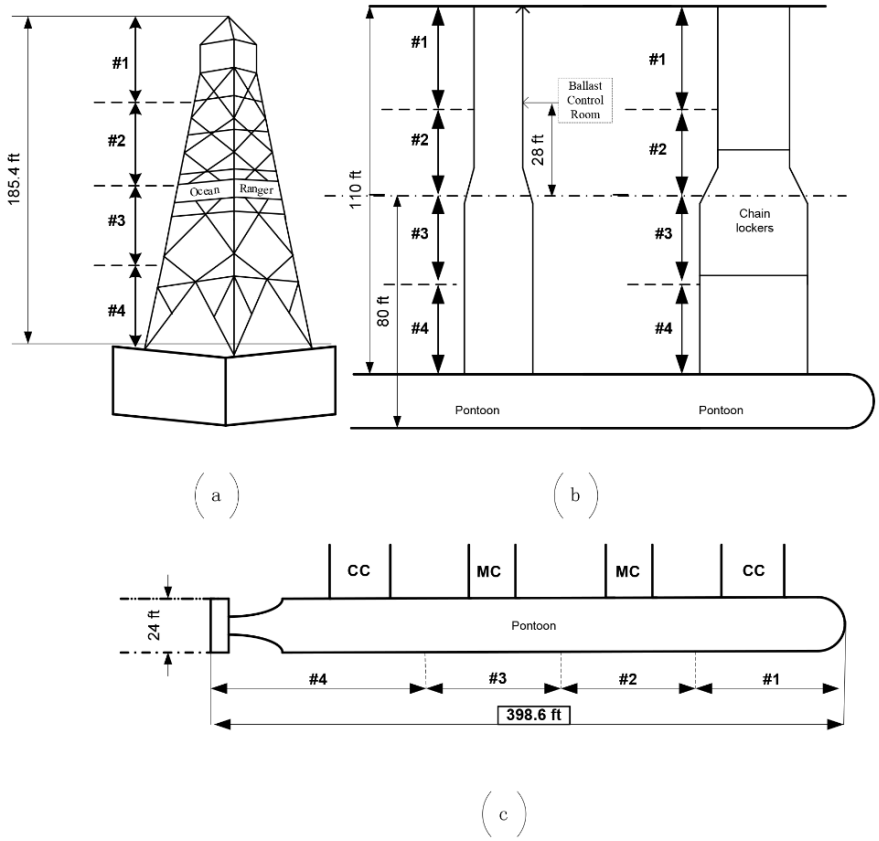

Figure 2-7. Schematic of the Ocean Ranger: derrick (a), middle and corner column (b) and pontoon (c) with generated sections

As a semi-submersible offshore drilling unit, the Ocean Ranger consisted of pontoons, derrick, supporting columns and main deck. Two pontoons, which contained drill water, ballast water and fuel, provided floatation and rig power for the unit. A total of eight columns consisting of four corner columns and four middle columns supported the deck, and were located port and starboard,

respectively. The ballast control room was in the starboard middle column 28 ft above the drilling draft, protected by deadlights. Two deck layers provided the living space for crew and work areas, above which was the 185.4-ft high drilling derrick. Figure 2-7 represents the generated structural units of the derrick, middle and corner columns, and pontoons. Similar to the demonstration example, four different sections are divided for derrick, corner column, and pontoons, while the Ocean Ranger had four more middle columns and the ballast control room was located at one of the middle columns. Noted that different components carry a diverse combination of loads, except for the derrick. In this paper, it is clarified that pontoons and columns under the operational draft suffer simultaneously from the damage of wave load and sea pressure. Columns above the water line and deck are buffeted by the combined impact of wave and wind loads. Ideally, the derrick should only be exposed to wind attacks. Results of a variety of loads for design, manufactured permissible condition and actual operating state are summarized in Table 2-5.

2.3.3 **Derive components' probabilities of failure under combined loads**

Probabilities of failure at components' levels under single loads can be solved by simultaneous equations of COV and substituting P and L in Equation (2.2) with an annual probability of exceedance 10^{-2} and operational payload (loads of affordable wind speed and wave height), respectively. It is assumed that the COV of every section statistically distributed wind resistance response is 0.036 and the COVs of statistically distributed wave resistance responses of corner column,

pontoon, deck and middle column are 0.15, 0.15, 0.30 and 0.20, respectively. The sea pressure acting on the pontoon is higher than columns due to deeper water, the COV of statistically distributed sea pressure resistance response of pontoon (0.014) is smaller than columns (0.017) for the sake of manufacture safety standards. Subsequently, Equation (2.3) uses the shape and location parameters of Equation (2.2) with the assumed correlation coefficient $\rho = 0$ (wind and wave independent assumption) to derive joint probabilities of failure for the joint combined load. The probabilities of failure for every component section are captured in Table 2-5.

As mentioned in the report (US Coast Guard, 1983), the deadlights, which should have protected the porthole from wave impact, were open because of improper operation. For this case, the strength reduction coefficient is introduced to model the damage probability of the portlight. At first, the portlights and the deadlights were regarded as a unit, designed and built to withstand 110-ft waves and 100-knot winds simultaneously. Because of the improper operation, the portlight was directly exposed to the harsh environments. Thus, the acceptable wave load of a portlight should be reassessed. Based on DNVGL-OS-C201 (2017), the specific minimum yield stress for normal strength steel is 235 MPa. However, the ultimate permissible load on the protected portlight is 36.92 KPa because of configuration and stress concentration. The maximum strength reduction coefficient is defined as the ratio of the specific minimum yield stress to the permissible load.

$$R_m = \frac{\sigma_m}{\sigma_P} = \frac{235MPa}{36.92\ KPa} = 6368.56 \qquad (2.8)$$

where σ_m is the specific minimum yield stress and σ_P is the permissible load.

The R_m is 6,368.56 for deadlights. For the sake of reliability and accuracy, 50% of the R_m is applied to the portlight, which is made of tempered glass. ASTM International (2018) stipulates the minimum surface compression for fully tempered glass is 69 MPa. Therefore, the permissible load for a portlight is 2.17×10^4 Pa, as is shown in Table 2-5.

2.3.4 **BN establishment and overall probabilities of failure estimation**

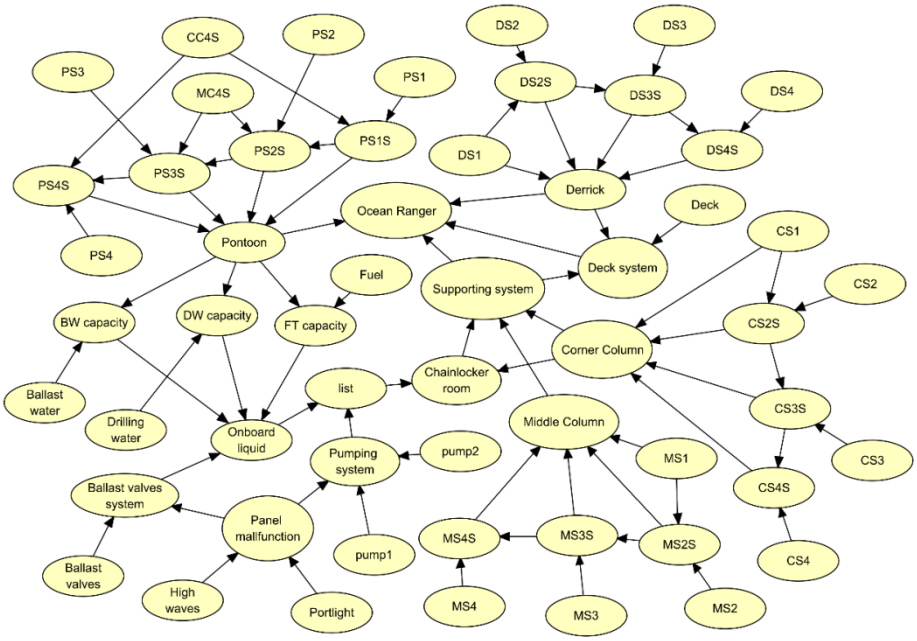

Figure 2-8. BN of operational failure modeling of the Ocean Ranger

It is worth pointing out that middle columns are taken into consideration because of the difference between the Ocean Ranger and the demonstration example. MS 1 – 4 represent the probabilities of failure of sections #1 to #4 of the middle column

caused by combined loads directly. MS2S represents both the direct damage and collateral debris damage from adjacent section #1 of the middle column. Damage to the derrick can destroy the deck due to objects falling from high altitudes. Furthermore, without the support of middle and corner columns, the supporting system cannot reinforce the deck. Columns are installed above the pontoons, which explains that once the sections of columns connected to the pontoons fails, related pontoon sections inevitably rupture. Then onboard liquid is influenced because it is stored in the pontoon which further manages the buoyancy of the SMU. Owing to a design flaw and improper operation, the ballast control room where the portlights are installed is under the height of wave crests, which leads to the failure of the deballast system. If the portlights are destroyed by a rogue wave, seawater can inundate the ballast control room, causing the panel malfunction. The panel which is protected by the portlight controls the pumping system and the ballast valves system, which thereby control the onboard liquid.

Finally, damage probability modeling of the Ocean Ranger considering stability and operational components is tailored in Figure 2-8 and Table 2-5 with CPTs provided in the Appendix. The probabilities of failure (PoF) of several aforementioned root nodes (Heising and Grenzebach, 1989), including valves, pumps, ballast water, drilling water, and fuel, were utilized to analyze failure probability using HUGIN 8.6 (http://www.hugin.com).

2.4 Results and Discussion

As can be seen from Table 2-5, wind load rises significantly along with the increase of height, which is calculated as 3.51 kPa for section #1 of the derrick,

while it is 1.69 kPa, almost half as much, for section #2 of columns. In general, the closer the height is to the sea horizon within a certain range, the greater roughness leads to wind's speed increasing with altitude.

Table 2-5 Nodes illustrations in Operational Failure Modeling of the Ocean Ranger

	Permissible Load			Actual Load			PoF
Component	Wind 10^3 Pa	Wave 10^4 Pa	Sea pressure 10^5 Pa	Wind 10^3 Pa	Wave 10^4 Pa	Sea pressure 10^5 Pa	
Derrick	-	-	-	-	-	-	7.00×10^{-4}
Section #1	3.51	-	-	2.84	-	-	1.89×10^{-4}
Section #2	3.33	-	-	2.69	-	-	1.59×10^{-4}
Section #3	3.11	-	-	2.52	-	-	2.20×10^{-4}
Section #4	2.82	-	-	2.28	-	-	1.74×10^{-4}
Deck	2.56	13.10	-	2.07	4.21	-	1.17×10^{-5}
Corner Col.	-	-	-	-	-	-	1.00×10^{-4}
Section #1	2.30	6.17	-	1.86	3.88	-	3.93×10^{-5}
Section #2	1.69	5.09	-	1.36	3.41	-	3.82×10^{-5}
Section #3	-	4.32	4.24	-	2.88	3.75	1.73×10^{-7}
Section #4	-	3.69	5.15	-	2.44	4.66	6.32×10^{-5}
Middle Col.	-	-	-	-	-	-	1.00×10^{-4}
Section #1	2.30	4.13	-	1.86	2.10	-	2.53×10^{-5}
Section #2	1.69	3.30	-	1.36	1.79	-	2.39×10^{-5}
Section #3	-	2.85	4.24	-	1.63	3.75	1.55×10^{-7}
Section #4	-	2.49	5.15	-	1.48	4.66	7.37×10^{-5}
Portlight	-	2.17	-	-	2.02	-	0.9757

Pontoons	-	-	-	-	-	-	2.00×10^{-4}
Section #1	-	5.58	6.00	-	3.67	5.51	2.74×10^{-5}
Section #2	-	5.58	6.00	-	3.67	5.51	2.74×10^{-5}
Section #3	-	5.58	6.00	-	3.67	5.51	2.74×10^{-5}
Section #4	-	5.58	6.00	-	3.67	5.51	2.74×10^{-5}
Ocean Ranger	-	-	-	-	-	-	0.7812

Moreover, the average failure probability of sections for the derrick is 1.86×10^{-4}. However, the average failure probabilities of sections for the deck, columns, and pontoons are approximately 1.17×10^{-5}, 3.30×10^{-5} and 2.74×10^{-5}. In this regard, derrick section experienced a relatively high probability of failure by almost one order of magnitude when compared to the other structural components. In spite of the mutual interaction of adjacent sections owing to the debris trajectory, the failure probability of the derrick, 7×10^{-4}, is still higher than for columns, 1×10^{-4}, and pontoons, 2×10^{-4}. The explanation for this phenomenon can be found through the application of bivariate joint probability distribution associated with the physical reliability model. Two different indicators are combined, which is more accordant with the actual situation than combining various types of loads directly. In other words, it is dominated by the parameter which is closer to the maximum value and influenced by the other one. In fact, deck, columns and pontoons suffer the impact from either the wind-wave combined load or wave-sea pressure combined load. Ideally, the derrick bears only the wind-induced load. In this case, the wind speed was 90 knots, which reached 90% of the maximum critical value and the wave height was 65 ft, only accounting for 59% of the limit. Thus, wind speed in the

prevailing conditions was the dominant indicator resulting in the derrick having a considerably high failure probability, while the wave height that was far beyond the limit was the influenced parameter. Therefore, components that bore either the load caused by the wave itself or the indirect dynamic sea pressure of each section were less likely to fail.

Along with this line of consideration, the simulation results in Table 2-5 indicate that the Ocean Ranger operated with an incredible probability of failure of 0.7812. This is around 78 times as large as the lower limit of the operational failure envelope. Logically speaking, if the estimated failure probability in the envelope fell dramatically, termination of the operation to cease the risk should have been adopted. On the contrary, probabilities of failure for the main structural components such as the derrick, middle and corner columns, pontoons, etc. were about 10^{-4}. The calculated failure probability was still acceptable, which proved that the Ocean Ranger could have survived the storm.

Nevertheless, due to inappropriate manual operations, the hurricane on 14/15 February 1982 destroyed the Ocean Ranger, unfortunately. As an improper operating procedure, the deadlights, which should have protected the porthole from wave impact, were open. As revealed by the reduction coefficient, the permissible load of the portlight decreased significantly from 3.30×10^4 Pa to 2.17×10^4 Pa. What is even worse, the actual imposed load was 2.02×10^4 Pa, which led ineluctably to the increase of probability of failure. The failure probability of the exposed portlight was derived as 0.9757, which is nearly 41,000 times greater than is the case under protection. Subsequently, the branch which follows the panel malfunction, failure of the pumping system and ballast valves,

severe listing, flooding of the chain locker and failure of the support system occurred naturally. Because of the unexpected flooding of the chain locker room, the failure probability of the supporting system rose sharply from 2×10^{-4} to 0.7810.

It is highlighted that the damage to the portlight which lacked the protection of deadlights initiated the chain of events, in agreement with the Marine Casualty Report (US Coast Guard, 1983). This signifies that in the actual operational process, not only do the design and manufacturing characteristics of the platform need to be taken into consideration, but also that human operation practices can add considerable additional risk to the platform. Aiming to lower the damage caused by improper manual operation from the inherent design to emergency actions is essential. If feasible, it is recommended to strengthen the training, knowledge, and instruction for proper operational procedures to enhance reliability and mitigate potential hazards.

2.5 Conclusions

The proposed operational failure model is able to capture real-time weather data and their impact on safe operation, which helps to promote safe and reliable offshore development. It is highlighted that this study assesses the operational risk of the semi-submersible mobile unit (SMU) quantitatively under combined wind and wave induced loads with a probabilistic Bayesian network (BN) framework, which represents conditional dependencies of the weather's effect. More specifically, it presents a detailed operational failure model considering the

combined loading of extreme weather conditions and the operational characteristics of the SMU. Consistent and reliable results are provided, as evidenced by the case study. As an anticipated risk estimation model, it is proved that the proposed model is a useful and reliable tool to develop and monitor an operational failure envelope of the SMU in given environmental conditions. For the sake of improvement, it is recommended that more environmental loads such as currents and sea ice induced loads should be taken into consideration to simulate the operational disturbance for further research.

This paper has demonstrated the application of wind load response modeling, the Morison model and the ultimate limit states method to estimate the combined loading of extreme weather conditions imposed on the SMU. A physical reliability model and joint probability distribution function have been incorporated, which provide a deeper insight to capture the risk response. Along with reducing the estimated failure probability through the implementation of BN with the operational failure envelope in given environmental conditions, further operational recommendations are suggested in order to avoid catastrophic disaster.

2.6 References

Abaei, M.M., Abbassi, R., Garaniya, V., Chai, S., Khan, F., 2018. Reliability assessment of marine floating structures using Bayesian network. Applied Ocean Research 76, 51-60.

Abaei, M.M., Arzaghi, E., Abbassi, R., Garaniya, V., Chai, S., Khan, F., 2018. A robust risk assessment methodology for safety analysis of marine structures under storm conditions. Ocean Engineering 156, 167-178.

ASTM International, 2018. ASTM C1048-18 Standard Specification for Heat-Strengthened and Fully Tempered Flat Glass. ASTM International. https://doi.org/10.1520/C1048-18.

Banks, M., Abdussamie, N., 2017. The response of a semisubmersible model under focused wave groups: Experimental investigation. Journal of Ocean Engineering and Science 2 (3), 161-171.

Barua, S., Gao, X., Pasman, H., Mannan, M.S., 2016. Bayesian network based dynamic operational risk assessment. Journal of Loss Prevention in the Process Industries 41, 399-410.

Bea, R., Iversen, R., Xu, T., 2001. Wave-in-deck forces on offshore platforms. Journal of offshore mechanics and arctic engineering 123 (1), 10-21.

Cheng, E., Yeung, C., 2002. Generalized extreme gust wind speeds distributions. Journal of Wind Engineering and Industrial Aerodynamics 90 (12-15), 1657-1669.

DNVGL-OS-C101, Design of offshore steel structures, general - LRFD method. July 2019. DNV GL

DNVGL-OS-C201, Structural design of offshore units - WSD method. July 2017. DNV GL

DNVGL-RP-C103, Column-Stabilised Units. July 2015. DNV GL

DNVGL-RP-C205, Enviromental conditions and enviromental loads. August 2017. DNV GL

Forbes, C., Evans, M., Hastings, N., Peacock, B., 2011. Statistical distributions. 4th ed. John Wiley & Sons, New Jersey, USA.

Ghafari, H., Dardel, M., 2018. Parametric study of catenary mooring system on the dynamic response of the semi-submersible platform. Ocean Engineering 153, 319-332.

Gomathinayagam, S., Vendhan, C., Shanmugasundaram, J., 2000. Dynamic effects of wind loads on offshore deck structures—a critical evaluation of provisions and practices. Journal of Wind Engineering and Industrial Aerodynamics 84 (3), 345-367.

Heising, C.D., Grenzebach, W.S., 1989. The ocean ranger oil rig disaster: A risk analysis. Risk analysis 9 (1), 55-62.

Holmes, J.D., 2015. Wind loading of structures. CRC press, 3rd ed, Florida, USA.

HUGIN Expert Software Version 8.6, 2017. http://www.hugin.com.

Ismail, Z., Kong, K.K., Othman, S.Z., Law, K.H., Khoo, S.Y., Ong, Z.C., Shirazi, S.M., 2014. Evaluating accidents in the offshore drilling of petroleum: Regional picture and reducing impact. Measurement 51, 18-33.

Kaplan, J., DeMaria, M., 1995. A simple empirical model for predicting the decay of tropical cyclone winds after landfall. Journal of applied meteorology 34 (11), 2499-2512.

Khakzad, N., Khan, F., Amyotte, P., 2012. Dynamic risk analysis using bow-tie approach. Reliability Engineering & System Safety 104, 36-44.

Lee, J.-c., Jeong, J.-h., Wilson, P., Lee, S.-s., Lee, T.-k., Lee, J.-H., Shin, S.-c., 2018. A study on multi-objective optimal design of derrick structure: Case study. International Journal of Naval Architecture and Ocean Engineering 10 (6), 661-669.

Leimeister, M., Kolios, A., 2018. A review of reliability-based methods for risk analysis and their application in the offshore wind industry. Renewable and Sustainable Energy Reviews 91, 1065-1076.

Liu, H., Sun, L., Huang, A., Zhao, Y., Chen, G., 2018. Performance-Based Analysis of Wind-Survivability for Large Offshore Jacket Platforms Subject to Hurricane, Paper Presented at the ASME 2018 37th International Conference on Ocean, Offshore and Arctic Engineering. American Society of Mechanical Engineers, Madrid, Spain.

Ma, J., Zhou, D., Han, Z., 2017. Wind and waves induced dynamic effects of a semi-submersible platform, Paper Presented at the 27th International Ocean and Polar Engineering Conference. International Society of Offshore and Polar Engineers, San Francisco, USA.

Ma, J., Zhou, D., Han, Z., Zhang, K., Bao, Y., Dong, L., 2019. Fluctuating wind and wave simulations and its application in structural analysis of a semi-submersible offshore platform. International Journal of Naval Architecture and Ocean Engineering 11 (1), 624-637.

Ma, J., Zhou, D., Han, Z., Zhang, K., Nguyen, J., Lu, J., Bao, Y., 2017. Numerical simulation of fluctuating wind effects on an offshore deck structure. Shock and

Vibration. p. 3210271.

Song, G., Khan, F., Wang, H., Leighton, S., Yuan, Z., Liu, H., 2016. Dynamic occupational risk model for offshore operations in harsh environments. Reliability Engineering & System Safety 150, 58-64.

US Coast Guard, 1983. Marine Casualty Report: Mobile Offshore Drilling Unit (MODU) Ocean Ranger, o.n. 615641 Capsizing and Sinking in the Atlantic Ocean, on 15 February 1982 with Multiple Loss of life (No. USCG 16732/0001). U.S. Department of Transportation, Washington, D.C.

Weber, P., Medina-Oliva, G., Simon, C., Iung, B., 2012. Overview on Bayesian networks applications for dependability, risk analysis and maintenance areas. Engineering Applications of Artificial Intelligence 25 (4), 671-682.

Yeo, C., Bhandari, J., Abbassi, R., Garaniya, V., Chai, S., Shomali, B., 2016. Dynamic risk analysis of offloading process in floating liquefied natural gas (FLNG) platform using Bayesian Network. Journal of Loss Prevention in the Process Industries 41, 259-269.

Yu, Y., Hardowar, A., Yu, J., Hao, S., Gao, X., 2018. Investigation of TLP's hydrodynamic response with different tendon connection angles. Theoretical and Applied Mechanics Letters 8 (4), 291-297.

Zhang, S. (2017, August 25). When a hurricane hits an offshore oil platform: Harvey could seriously damage oil and gas operations in the Gulf of Mexico. The Atlantic: Science Edition Retrieved from: https://www.theatlantic.com/science/archive/2017/08/harvey-offshore-platform-oil-gas/537960/

2.7 Appendix

The subjective belief is adapted to assign CPTs to reduce uncertainty, which is sufficient to estimate the anticipated operational probability of failure for the purpose of a safety reference. In short, the greater the height of the section, the greater the mutual influence factor is, since the uppermost section has a strongest potential of both kinetic and gravitational. Furthermore, it is assumed that only two adjacent sections interact with the debris trajectory. As a consequence, Table 2-6 - Table 2-22 show the CPTs of the developed BN ($\bar{x_i}$ represents the damage/occurrence of component x_i and W represents working condition, F represents failure).

Table 2-6 The CPT of section #2, #3 and #4 for the derrick

#2	DS1		$\overline{DS1}$		#3	DS2S		$\overline{DS2S}$		#4	DS3S		$\overline{DS3S}$	
	DS2	$\overline{DS2}$	DS2	$\overline{DS2}$		DS3	$\overline{DS3}$	DS3	$\overline{DS3}$		DS4	$\overline{DS4}$	DS4	$\overline{DS4}$
DS2S	1	0	0.49	0	DS3S	1	0	0.57	0	DS4S	1	0	0.65	0
$\overline{DS2S}$	0	1	0.51	1	$\overline{DS3S}$	0	1	0.43	1	$\overline{DS4S}$	0	1	0.35	1

Table 2-7 The CPT for the derrick

	DS1								$\overline{DS1}$							
	DS2S				$\overline{DS2S}$				DS2S				$\overline{DS2S}$			
	DS3S		$\overline{DS3S}$		DS3S		$\overline{DS3S}$		DS3S		$\overline{DS3S}$		DS3S		$\overline{DS3S}$	
DS4S	w	F	w	F	w	F	w	F	w	F	w	F	w	F	w	F
Derrick	1	0	0	0	0	0	0	0	0	0	0	0	0	0	0	0
$\overline{Derrick}$	0	1	1	1	1	1	1	1	1	1	1	1	1	1	1	1

Table 2-8 The CPT for the deck

	Supporting system				$\overline{\text{Supporting system}}$			
	Derrick		$\overline{\text{Derrick}}$		Derrick		$\overline{\text{Derrick}}$	
	Deck	$\overline{\text{Deck}}$	Deck	$\overline{\text{Deck}}$	Deck	$\overline{\text{Deck}}$	Deck	$\overline{\text{Deck}}$
DECKS	1	0	0.68	0	0.59	0	0.24	0
$\overline{\text{DECKS}}$	0	1	0.32	1	0.41	1	0.76	1

Table 2-9 The CPT of section #2, #3 and #4 for the corner column

#2	CS1		$\overline{\text{CS1}}$		#3	CS2S		$\overline{\text{CS2S}}$		#4	CS3S		$\overline{\text{CS3S}}$	
	CS2	$\overline{\text{CS2}}$	CS2	$\overline{\text{CS2}}$		CS3	$\overline{\text{CS3}}$	CS3	$\overline{\text{CS3}}$		CS4	$\overline{\text{CS4}}$	CS4	$\overline{\text{CS4}}$
CS2S	1	0	0.52	0	CS3S	1	0	0.64	0	CS4S	1	0	0.72	0
$\overline{\text{CS2S}}$	0	1	0.48	1	$\overline{\text{CS3S}}$	0	1	0.36	1	$\overline{\text{CS4S}}$	0	1	0.28	1

Table 2-10 The CPT for the corner column

	CS1								$\overline{\text{CS1}}$							
	CS2S				$\overline{\text{CS2S}}$				CS2S				$\overline{\text{CS2S}}$			
	CS3S		$\overline{\text{CS3S}}$		CS3S		$\overline{\text{CS3S}}$		CS3S		$\overline{\text{CS3S}}$		CS3S		$\overline{\text{CS3S}}$	
CS4S	w	F	w	F	w	F	w	F	w	F	w	F	w	F	w	F
Corner column	1	0	0	0	0	0	0	0	0	0	0	0	0	0	0	0
$\overline{\text{Corner column}}$	0	1	1	1	1	1	1	1	1	1	1	1	1	1	1	1

Table 2-11 The CPT for the supporting system

	Chainlocker room				$\overline{\text{Chainlocker room}}$			
	Middle column		$\overline{\text{Middle column}}$		Middle column		$\overline{\text{Middle column}}$	
Corner column	w	F	w	F	w	F	w	F
Supporting system	1	0	0	0	0	0	0	0
$\overline{\text{Supporting system}}$	0	1	1	1	1	1	1	1

Table 2-12 The CPT of section #2, #3 and #4 for the middle column

#2	MS1		$\overline{\text{MS1}}$		#3	MS2S		$\overline{\text{MS2S}}$		#4	MS3S		$\overline{\text{MS3S}}$	
	MS2	$\overline{\text{MS2}}$	MS2	$\overline{\text{MS2}}$		MS3	$\overline{\text{MS3}}$	MS3	$\overline{\text{MS3}}$		MS4	$\overline{\text{MS4}}$	MS4	$\overline{\text{MS4}}$
MS2S	1	0	0.54	0	MS3S	1	0	0.66	0	MS4S	1	0	0.74	0
$\overline{\text{MS2S}}$	0	1	0.46	1	$\overline{\text{MS3S}}$	0	1	0.34	1	$\overline{\text{MS4S}}$	0	1	0.26	1

Table 2-13 The CPT for the middle column

	MS1								$\overline{\text{MS1}}$							
	MS2S				$\overline{\text{MS2S}}$				MS2S				$\overline{\text{MS2S}}$			
	MS3S		$\overline{\text{MS3S}}$		MS3S		$\overline{\text{MS3S}}$		MS3S		$\overline{\text{MS3S}}$		MS3S		$\overline{\text{MS3S}}$	
MS4S	w	F	w	F	w	F	w	F	w	F	w	F	w	F	w	F
Middle column	1	0	0	0	0	0	0	0	0	0	0	0	0	0	0	0
$\overline{\text{Middle column}}$	0	1	1	1	1	1	1	1	1	1	1	1	1	1	1	1

Table 2-14 The CPT for the chainlocker room and the ballast valves system

Chainlocker room	Corner column		$\overline{\text{Corner column}}$		Ballast valves system	Ballast valves		$\overline{\text{Ballast valves}}$	
	List	$\overline{\text{list}}$	List	$\overline{\text{list}}$		Panel	$\overline{\text{Panel}}$	Panel	$\overline{\text{Panel}}$
Chainlocker room	1	0	0	0	Ballast valves system	1	0	0	0
$\overline{\text{Chainlocker room}}$	0	1	1	1	$\overline{\text{Ballast valves system}}$	0	1	1	1

Table 2-15 The CPT for the onboard liquid

	Ballast valves system								$\overline{\text{Ballast valves system}}$							
Ballast water capacity	w				F				w				F			
Fuel tank capacity	w		F		w		F		w		F		w		F	
Drilling water capacity	w	F	w	F	w	F	w	F	w	F	w	F	w	F	w	F
Onboard liquid	1	0	0	0	0	0	0	0	0	0	0	0	0	0	0	0
$\overline{\text{Onboard liquid}}$	0	1	1	1	1	1	1	1	1	1	1	1	1	1	1	1

Table 2-16 The CPT for the drilling water capacity and ballast water capacity

	Pontoon		$\overline{\text{Pontoon}}$			Pontoon		$\overline{\text{Pontoon}}$	
	Ballast wa	$\overline{\text{Ballast wa}}$	Ballast wa	$\overline{\text{Ballast wa}}$		Drilling wa	$\overline{\text{Drilling wa}}$	Drilling wa	$\overline{\text{Drilling wa}}$
BWC	1	0	0	0	DWC	1	0	0	0
$\overline{\text{BWC}}$	0	1	1	1	$\overline{\text{DWC}}$	0	1	1	1

Table 2-17 The CPT for the fuel tank capacity and section #1 for the pontoon

	Pontoon		$\overline{\text{Pontoon}}$			CC4S		$\overline{\text{CC4S}}$	
	Fuel	$\overline{\text{Fuel}}$	Fuel	$\overline{\text{Fuel}}$		PS1	$\overline{\text{PS1}}$	PS1	$\overline{\text{PS1}}$

Fuel tank capacity	1	0	0	0	PS1S	1	0	0.55	0
$\overline{\text{Fuel tank capacity}}$	0	1	1	1	$\overline{\text{PS1S}}$	0	1	0.45	1

Table 2-18 The CPT of section #2 for the pontoon

	MC4S				$\overline{\text{MC4S}}$			
	PS1S		$\overline{\text{PS1S}}$		PS1S		$\overline{\text{PS1S}}$	
	PS2	$\overline{\text{PS2}}$	PS2	$\overline{\text{PS2}}$	PS2	$\overline{\text{PS2}}$	PS2	$\overline{\text{PS2}}$
PS2S	1	0	0.48	0	0.67	0	0.25	0
$\overline{\text{PS2S}}$	0	1	0.52	1	0.33	1	0.75	1

Table 2-19 The CPT of section #3 and #4 for the pontoon

#3	MC4S				$\overline{\text{MC4S}}$				#4	CC4S				$\overline{\text{CC4S}}$			
	PS2S		$\overline{\text{PS2S}}$		PS2S		$\overline{\text{PS2S}}$			PS3S		$\overline{\text{PS3S}}$		PS3S		$\overline{\text{PS3S}}$	
	PS3	$\overline{\text{PS}}$	PS3	$\overline{\text{PS3}}$	PS3	$\overline{\text{PS}}$	PS3	$\overline{\text{PS3}}$		PS4	$\overline{\text{PS4}}$	PS4	$\overline{\text{PS4}}$	PS4	$\overline{\text{PS4}}$	PS4	$\overline{\text{PS4}}$
PS3S	1	0	0.48	0	0.67	0	0.25	0	PS4S	1	0	0.48	0	0.55	0	0.08	0
$\overline{\text{PS3S}}$	0	1	0.52	1	0.33	1	0.75	1	$\overline{\text{PS4S}}$	0	1	0.52	1	0.45	1	0.92	1

Table 2-20 The CPT for the pontoon

	PS1S								$\overline{\text{PS1S}}$							
	PS2S				$\overline{\text{PS2S}}$				PS2S				$\overline{\text{PS2S}}$			
	PS3S		$\overline{\text{PS3S}}$		PS3S		$\overline{\text{PS3S}}$		PS3S		$\overline{\text{PS3S}}$		PS3S		$\overline{\text{PS3S}}$	
PS4S	w	F	w	F	w	F	w	F	w	F	w	F	w	F	w	F
Pontoon	1	0	0	0	0	0	0	0	0	0	0	0	0	0	0	0
$\overline{\text{Pontoon}}$	0	1	1	1	1	1	1	1	1	1	1	1	1	1	1	1

Table 2-21 The CPT for the pumping system

	Panel				$\overline{\text{Panel}}$			
	Pump 1		$\overline{\text{Pump 1}}$		Pump 1		$\overline{\text{Pump 1}}$	
	Pump 2	$\overline{\text{Pump2}}$	Pump 2	$\overline{\text{Pump2}}$	Pump 2	$\overline{\text{Pump2}}$	Pump 2	$\overline{\text{Pump2}}$
Pumping system	1	1	1	0	0	0	0	0
$\overline{\text{Pumping system}}$	0	0	0	1	1	1	1	1

Table 2-22 The CPT for the Ocean Ranger

	Pontoon								$\overline{\text{Pontoon}}$							
Supporting system	w				F				w				F			
Derrick	w		F		w		F		w		F		w		F	
Deck system	w	F	w	F	w	F	w	F	w	F	w	F	w	F	w	F
Ocean ranger	1	0	0	0	0	0	0	0	0	0	0	0	0	0	0	0
$\overline{\text{Ocear ranger}}$	0	1	1	1	1	1	1	1	1	1	1	1	1	1	1	1

Chapter 3. Monitoring and Modeling of Environmental Load Considering Dependence and Its Impact on the Failure Probability[2]

Jinjie Fu and Faisal Khan*

Centre for Risk, Integrity and Safety Engineering (C-RISE),

Faculty of Engineering and Applied Science,

Memorial University of Newfoundland, St. John's, NL, A1B 3X5, Canada

Abstract

Extreme weather conditions put heavy environmental loads on systems and may cause catastrophic failure. Classification societies such as Lloyd's Register, DNV GL and the American Bureau of Shipping recommend methods for environmental load calculations. These methods do not consider dependencies among parameters when calculating environmental loads. This paper proposes a novel methodology to consider the copula-based bivariate failure function to evaluate the dependence structure of parameters and minimize uncertainty in load calculations. It also presents a robust operational failure assessment model that considers real-time environmental parameters along with their dependencies. The proposed methodology and models are tested on a semi-submersible mobile unit (SMU).

[2] Fu, J., & Khan, F. Monitoring and modeling of environmental load considering dependence and its impact on the failure probability. Submitted to Ocean Engineering.

The failure probability corresponding to the wind and wave loads imposed on the SMU is calculated using a physical reliability model and Bayesian network. The copula-based bivariate failure function defines the dependence using the parameters δ, which are estimated using maximum likelihood estimation. A detailed case study illustrates the advantage of the proposed methodology. The proposed method is of vital significance to developing a safe operating envelope for offshore assets likely to face extreme weather conditions.

Keywords: Operational failure; Environmental loads; Dependence; Copula function; Maximum likelihood estimation

3.1 Introduction

Hurricanes have become more frequent in the past few decades. In the 2005 Atlantic hurricane season, for example, the number of hurricanes recorded that year, 15, broke the annual record set in 1969 [1]. The property damage and economic losses that result from the landfall of hurricanes have also become more severe. For example, Hurricane Katrina destroyed 44 offshore platforms [2] and shut down many of the oil and gas production facilities located in the Gulf of Mexico. Hence, research on environmental loads and their impact on the failure of systems is of great importance to avoiding personal injury and property loss.

Classification societies suggest employing standards to calculate environmental loads, such as those used by DNV GL [3] and the American Bureau of Shipping (ABS) [4]. These standards provide effective and accurate results, are widely applied, and have been proven to be effective in numerous engineering practices. Suja-Thauvin et al. [5] used DNV GL standards to develop a hydrodynamic load model that analyzes the mode response of a monopile offshore wind turbine. Caille et al. [6] adopted and validated a hydrodynamics model based on DNV GL methods for a tension leg platform (TLP) with inclined legs. Flis [7] applied the provisions of the ABS and calculated the environmental loads for cooling skid units. Li et al. [8] calculated wave loads in accordance with the ABS rules of a 7th generation semi-submersible drilling unit (CSDU) to optimize its structural configuration. However, the assessment of the dependencies among the parameters to calculate environmental loads is lacking. In the case of actual operation, these weather parameters have a certain interaction relationship,

particularly in harsh environments. This paper examines whether it underestimates or overestimates the impact on the failure of the system.

In regard to dependence construction, the copula function is an emerging model. Due to the complex interactions that occur in nature, the linear correlation coefficient lacks the ability to ascertain the dependence among real-time environmental parameters. The copulas overcome this limitation through the capacity to model any dependence structures, and they have been widely used in the field of financial investment, portfolio construction, and so on [9]. Recently, scholars have applied the copula function to system safety and reliability assessments [10-14]. Hashemi et al. [12] proposed a multivariate loss function that combined the marginal loss functions with copulas for process facilities risk analysis. Guo et al. [13] conducted a copula-based Bayesian network (CBBN) model to analyze the process system that addressed the limitations of non-linear dependence structures. Shen et al. [14] developed a mixed copula function to acquire the dependence details among failure modes to analyze the reliability of a gear door lock system. Here, the copula function is considered to propose an innovative operational failure assessment model because of its flexibility.

This work calculates environmental loads using real-time weather data and estimates the operational failure probability of the system. The dependence structure between the real-time environmental parameters is described with copula functions. The dependence parameters δ of the candidate copula models are estimated using maximum likelihood estimation. Then, the Akaike's information criterion (AIC) differences and Akaike weight are used to select the best copula

model to depict the dependence structure between the parameters to calculate the environmental loads. The comparison results of the case study demonstrate the flexibility and significance of the proposed model.

The structure of this paper is described as follows. Section 3.2 explains the procedure of the proposed real-time environmental load and its impact considering the dependence model with a simple illustrative example. Then, Section 3.3 applies the proposed model to a typical semi-submersible mobile unit (SMU) as a case study to demonstrate its general applicability. The results of the copula-based bivariate failure function and independent load failure function are compared and discussed in Section 3.4. The main findings of the study are summarized in Section 3.5.

3.2 The Proposed Methodology

The practical applicability of operational failure assessment with real-time weather observation is highlighted using a copula-based dependence function. The copula function defines the dependence between the parameters to calculate environmental loads in this paper. Figure 3-1 shows the details of the proposed methodology. The steps of the proposed methodology are explained with a simple example.

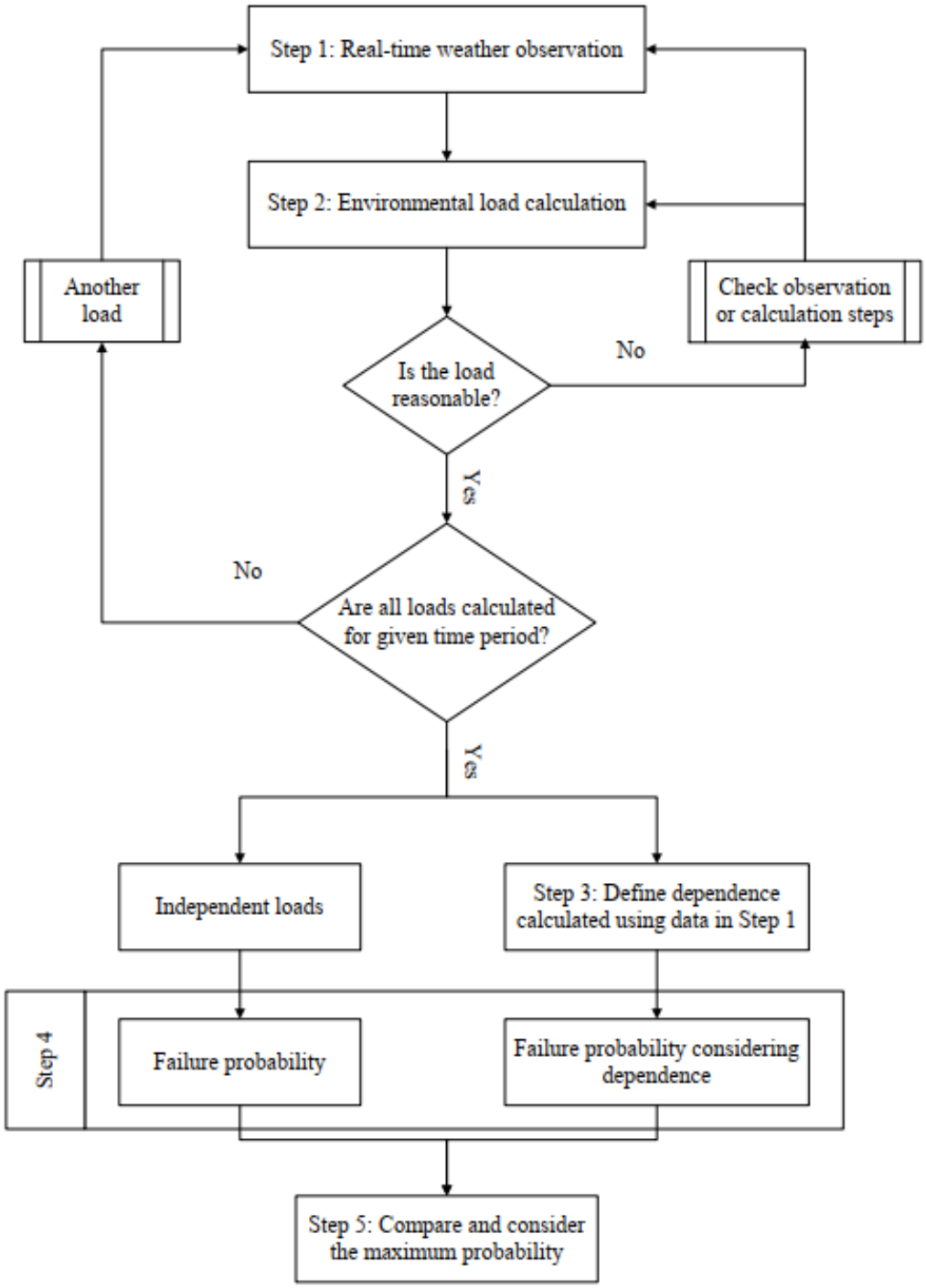

Figure 3-1. Real-time operational failure assessment methodology with copula-based dependence

3.2.1 Step 1: Real-time weather observation

As the basis of the proposed model, the first step is to gain access to real-time weather data. The environmental loads calculated in this paper are wind loads and wave loads. Therefore, 500 sets of wave data and concurrent meteorological observation data were obtained from wave data available online from the Department of Fisheries and Oceans Canada (DFO) [15]. Figure 3-2 plots an example with wind speed and wave height.

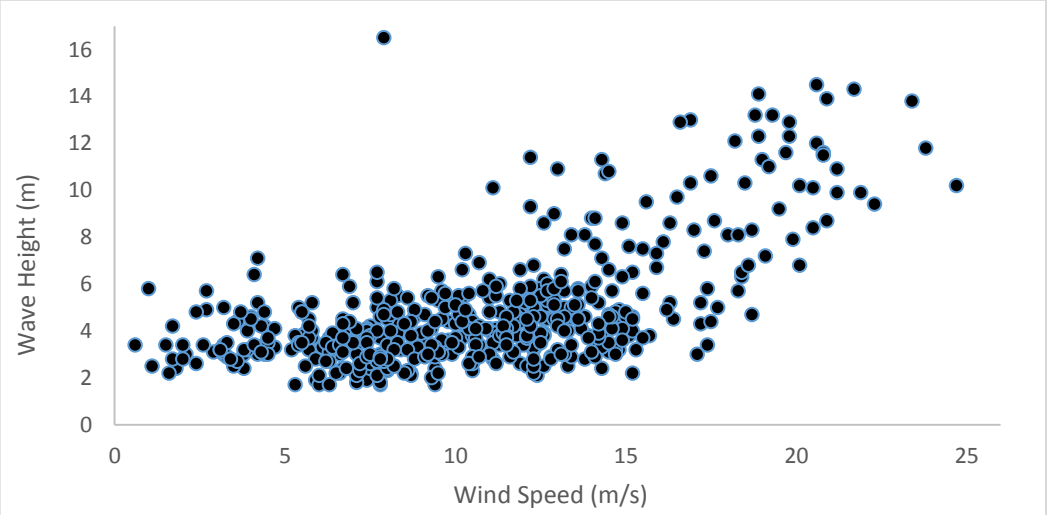

Figure 3-2. Scatter plot of the wind speed and wave height example

3.2.2 Step 2: Environmental load calculation

Once the real-time weather data are obtained, the environmental loads are calculated with the corresponding model. It is suggested from DNVGL-RP-C205 [3] that the wind and wave-induced loads are estimated from the wind load modeling and Morison wave load model, respectively.

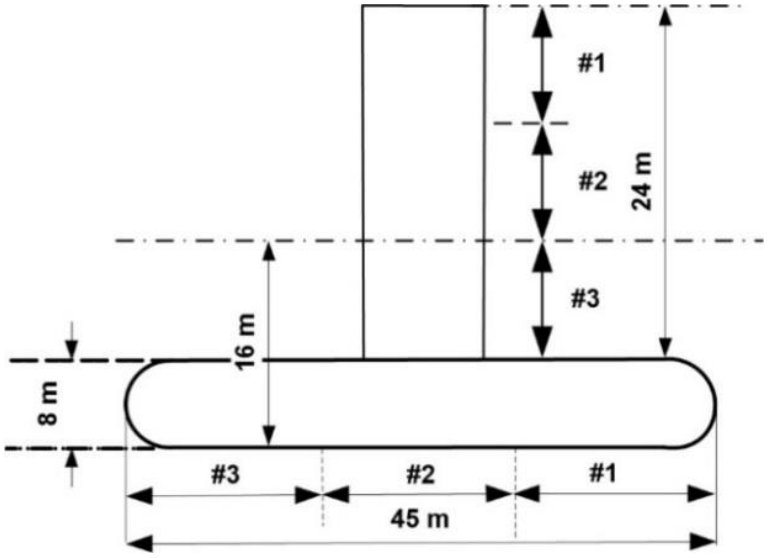

Figure 3-3. Schematic of the sample object with different sections

Table 3-1 shows the physical characteristics of the sample object. As revealed in Figure 3-3, the sample object is used to demonstrate the proposed methodology. The sample object consists of a pontoon and a column. The pontoon provides flotation to the system and supports other functional structure components, which are simplified as a column on the top of it. To further evaluate the impact of the environmental loads on the failure of the system, each structural component is divided into several sections that form the root causes of the Bayesian network (BN).

Table 3-1 Physical characteristics of the sample object

Component	Parameter	Value	Component	Parameter	Value
Column	Height	24 m	Pontoon	Height	8 m
	Diameter	10 m		Length	45 m

Waterline	Depth	16 m		Width	15 m
Winds	Maximum	30 m/s	Waves	Maximum	30 m

The sections for the column are trisected according to the height, as presented in Figure 3-3. Similarly, generated sections #1, #2 and #3 of the pontoon are divided by the length.

3.2.3 Step 3: Define dependence calculated using data in Step 1

Along this line of consideration, the procedure followed is the dependence assessment. The copula was first proposed by Sklar [16] in 1959 and is known as the theorem of Sklar. It has been shown that copula is a robust tool for assessing the dependence among random variables by establishing the joint distribution. Because it is a marginal distribution-free model, it is capable of capturing the dependence directly from the sample data. In other words, copula-based dependence assessment allows the combination of a variety of types of d-dimensional marginal distributions.

Here, the bivariate case is used to analyze the dependence structure between wind speed and wave height, which are the dominant parameters used to calculate the wind loads and wave loads, respectively.

$$F(x_1, x_2) = C(F_1(x_1), F_2(x_2)) \tag{3.1}$$

The joint distribution function is expressed in Equation (3.1). Two random variables are represented as x_1 and x_2. Then, the copula function C is written in Equation (3.2).

$$C(\mu_1, \mu_2) = F\left(F_1^{-1}(\mu_1), F_2^{-1}(\mu_2)\right) = \int_{-\infty}^{\mu_1} \int_{-\infty}^{\mu_2} c(x, y) dx dy \quad (3.2)$$

Where, $c(x, y)$ is the density of the copula.

Compared with implicit copulas such as Gaussian copula, Archimedean copula family [17] are defined as explicit copulas with simple closed forms. This makes them suitable for low-dimensional joint distribution. Three examples of Archimedean copulas [18] are the Clayton copula, the Frank copula and the Gumbel copula.

$$C_{Clayton}(\mu_1, \mu_2) = \left({\mu_1}^{-\delta} + {\mu_2}^{-\delta} - 1\right)^{-\frac{1}{\delta}} \quad (3.3)$$

Where, $\delta \in [-1, \infty) \setminus \{0\}$.

$$C_{Frank}(\mu_1, \mu_2) = -\frac{1}{\delta} ln(1 + \frac{(e^{-\delta\mu_1} - 1)(e^{-\delta\mu_2} - 1)}{e^{-\delta} - 1}) \quad (3.4)$$

Where, $\delta \in (-\infty, \infty) \setminus \{0\}$.

$$C_{Gumbel}(\mu_1, \mu_2) = exp\left\{-((-ln(\mu_1))^{\delta} + (-ln(\mu_2))^{\delta})^{\frac{1}{\delta}}\right\} \quad (3.5)$$

Where, $\delta \in [1, \infty)$.

δ explains the dependence information between the random variables μ_1 and μ_2. The Clayton copula, the Frank copula, and the Gumbel copula have lower tail dependence, radial symmetry, and upper tail dependence, respectively. Therefore, nearly all the tail dependences can be estimated by the three copula candidate models.

Logically, the next thing to do is to determine the parameters δ efficiently and precisely. The canonical maximum likelihood method (CML) [19] is introduced here. The main advantage of the copula function is that the error caused by the

improper choice of the marginal distributions can be avoided. The semiparametric method CML satisfies the goal of estimating the parameters δ directly from the data sets.

The copula density is used to calculate the pseudo log-likelihood function. Symbolic expressions of the bivariate copula density for the three candidate models are addressed with the help of MATLAB [20]. For example, the copula density for the Clayton copula is shown in Equation (3.6).

$$c(\mu_1, \mu_2) = \frac{\partial^2 C_{Clayton}(\mu_1,\mu_2)}{\partial \mu_1 \partial \mu_2} = (1+\delta)(\mu_1\mu_2)^{-\delta-1}\left({\mu_1}^{-\delta} + {\mu_2}^{-\delta} - 1\right)^{-\frac{1}{\delta}-2} \quad (3.6)$$

Following this, μ_1 and μ_2 are the uniform marginal variates. It can be solved by the rescaled empirical distribution function by means of the indicator function, as is shown in Equation (3.7).

$$\mu = F(x) = \frac{\sum_{i=1}^{n} 1(X_i \leq x)}{n+1} \quad (3.7)$$

Where n is the sample data size.

Ultimately, the parameter δ is confirmed by forming and maximizing the pseudo log-likelihood function (LLF), which is written in Equation (3.8).

$$\delta = arg\,max\,LLF(\delta) = \sum_{i=1}^{n} ln(c(\mu_1, \mu_2)) \quad (3.8)$$

For the sake of method demonstration, the dependence function between the wind speed and wave height in Figure 3-2 is used as an example application. Figure 3-4 presents the transformed data sample results using the rescaled empirical distribution function.

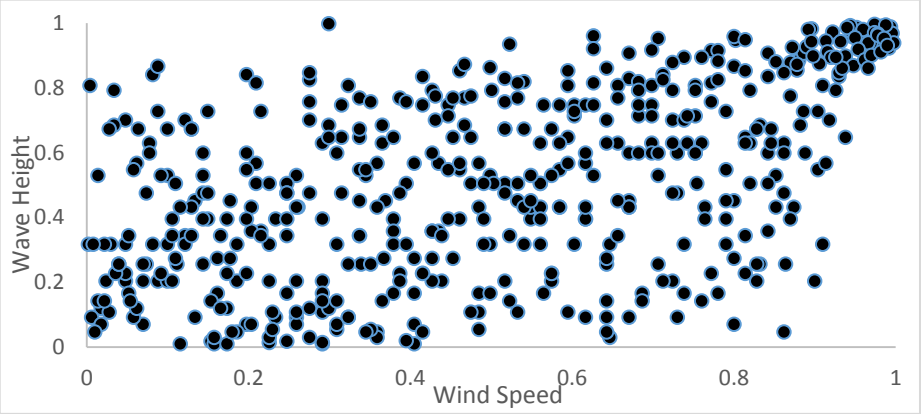

Figure 3-4. Scatter plot of wind speed and wave height after uniform transformation

Although the parameters δ are estimated by the CML, the specification of the most suitable copula function should be clarified. Hashemi et al. [12] recommended application of the Akaike's information criterion (AIC) to select the best model among candidate copulas. As a comparison approach, AIC compares the distances between the candidate models and the real model, which are shown in Equation (3.9).

$$AIC = 2(P - LLF(\delta)) \tag{3.9}$$

Where P is the number of unknown parameters. In this paper, CML needs to estimate the parameters δ. Therefore, P equals 1. The differences between the distances of the candidate models and the real model and the corresponding Akaike weights are written in Equation (3.10) and (3.11)

$$\Delta_i = AIC_i - AIC_{min} \tag{3.10}$$

It is natural that the candidate model with the smallest Δ_i is the most suitable model. In other words, the greater the Δ_i, the further the distance between the candidate model and the best model.

$$w_i = \frac{exp(-0.5\Delta_i)}{\sum_{r=1}^{R} exp(-0.5\Delta_r)} \tag{3.11}$$

Another alternative selection method [21] is the Akaike weight w_i, where R is the number of candidate copulas. Thus, the weight w_i is influenced by the candidate number. The larger the w_i, the more evident it is that the corresponding model is the exact model.

Table 3-2 CML and model selection calculation results

Copula	$\boldsymbol{\delta}$	$\boldsymbol{LLF(\delta)}$	**AIC**	Δ_i	$\boldsymbol{w_i}$
Clayton	0.568	35.177	-68.354	144.878	0
Frank	3.786	80.878	-159.756	53.476	0
Gumbel	1.617	107.616	-213.232	0	1

Table 3-2 shows the example results calculated from the maximum log-likelihood function and best model selection methods: AIC differences and Akaike weights. As can be seen, the AIC differences and the Akaike weights show substantial evidence that the Gumbel copula model is sufficient to describe the dependence structure between the 500-set example for wind speed and wave height. Accordingly, the CML and AIC with associated AIC differences and Akaike weights are able to capture the dependence function among bivariate distributed

random variables. Therefore, it is suitable for assessing the dependence structure between the parameters to calculate the loads induced by wind and waves.

3.2.4 Step 4: Failure probability calculation

From Steps 1 to 3, the environmental loads and dependence structure between parameters used to calculate the environmental loads are clarified. Therefore, how to evaluate the imposed environmental loads of each section quantitatively with probabilities is of great significance.

Ebeling [22] put forward the physical reliability model, which can assess the failure probability of structures, mechanical facilities and so on. It is assumed that either stress or strengthen or both of them follow specific types of distributions. Each divided section is made up of many nodes, each of which has different resistances to wind-induced loads and wave-induced loads. The resistances should be no less than zero. Thus, it is assumed that both resistances to wind-induced loads and wave-induced loads of a particular section follow the lognormal distributions.

$$P(failure) = \int_0^L f_r(r)\, dr = \Phi(\frac{1}{s} ln \frac{L}{t_{med}}) \quad (3.12)$$

Equation (3.12) explains that the failure probability is calculated through the integration of the resistance from zero to the load. When the wind speed is $30\ \mathrm{m/s}$ or the wave height is $30\ \mathrm{m}$ (maximum design and manufactured environmental parameters for the sample object), the wind or wave loads correspond to the failure probabilities 10^{-2}, as recommended by DNVGL-OS-C101 [23]. The coefficient of variation (CV) is also used to derive the unknown

parameters of the lognormal distribution.

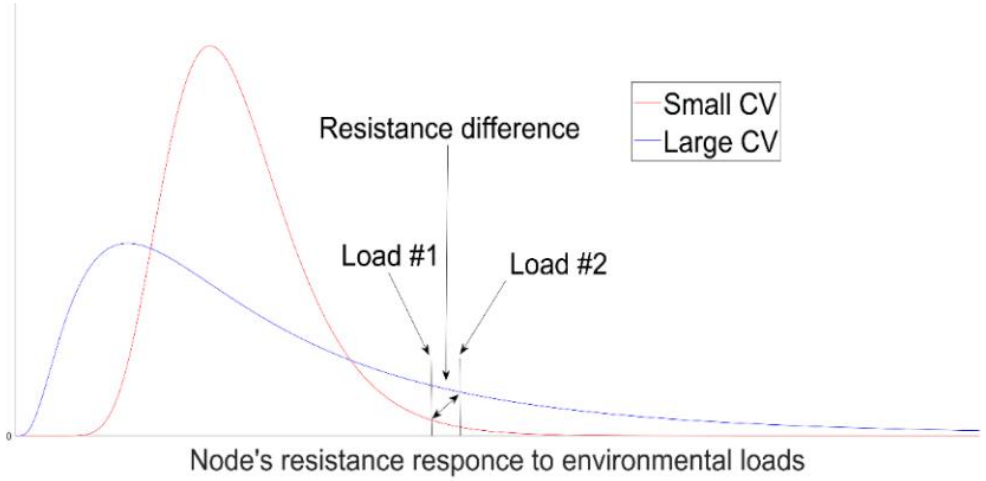

Figure 3-5. Node's resistance response to environmental loads with different CVs

Figure 3-5 shows the influence of the CV. Intuitively, the higher the CV, the more sensitive to the loads the section is. Robert Bea (a professor emeritus at the University of California, Berkeley) observed [24] that “cresting waves will do real damage” when compared to wind and rainfall. Thus, the CV of wave load resistance is greater than the CV of wind load resistance for the section under the impact of combined loads. In this example case, it is assumed that the CV of wave load resistance is 0.132 and the CV of wind load resistance is 0.108 for section #2 of the column. When compared to the pontoon and section #3 of the column, the wave forces imposed on section #3 are smaller. From the perspective of operation, the sample object has the ability to withstand the designed maximum wave height as a whole system, which means the column and pontoon are all in normal operating conditions. Therefore, the failure probabilities should be at a similar magnitude. It is assumed that the CV of wave load resistances for the pontoon and

section #3 of the column are 0.083 and 0.068, respectively, and the CV of wind load resistance for section #1 of the column is 0.101 for the sake of manufacture safety standards.

Table 3-3 Environmental loads for the sample object

Structure Level		Maximum Bearable Loads		Example loads	
Component	Section Number	Wind 10^2 Pa	Wave 10^4 Pa	Wind 10^2 Pa	Wave 10^4Pa
Column	#1	7.75	5.36	4.06	-
	#2	5.69	4.53	2.98	3.01
	#3	-	3.83	-	2.48
Pontoon	#1	-	5.17	-	3.05
	#2	-	5.17	-	3.05
	#3	-	5.17	-	3.05

Sample data (wind speed $21.7\ \mathrm{m/s}$, wave height $14.3\ \mathrm{m}$) from Figure 3-2 are used as example environmental parameters to calculate the environmental loads and failure probabilities. The results are shown in Table 3-3 and Table 3-4.

3.2.5 Step 5: Compare and consider the maximum probability of failure

The failure probabilities for every section are calculated through the physical reliability model, and the next step is to derive the failure probabilities from the

level of sections to the level of components and from the level of components to the system. Bayesian network (BN) is a causal inference model capable of integrating the overall probability with the help of nodes, arcs and conditional probability tables (CPTs) [25]. It is demonstrated in Figure 3-6 that root causes represent the failure probabilities from the level of sections. The arcs represent the causal relationships among nodes that are achieved mathematically by the CPTs.

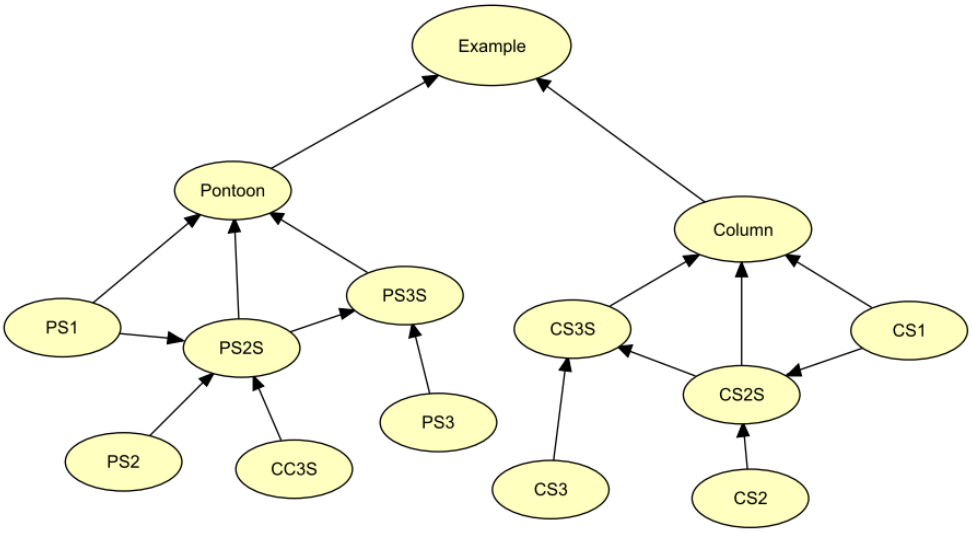

Figure 3-6. BN for the sample object

As mentioned before, the main structural components of the sample object include a column and pontoon. As shown in Figure 3-3, the pontoon and column have three sections, which are represented as PS1 – 3 and CS1 - 3. The suffix “S” refers to damage caused by debris from adjacent sections.

Table 3-4 Failure probabilities using the example sample data

Node	Probability	Node	Probability

Column Independent	7.12×10^{-5}	Pontoon	9.25×10^{-5}
Column Copula Dependent	6.00×10^{-4}	Section #1	2.68×10^{-5}
Section #1	2.18×10^{-5}	Section #2	2.68×10^{-5}
Section #2 Independent	2.58×10^{-5}	Section #3	2.68×10^{-5}
Section #2 Copula Dependent	5.96×10^{-4}	Sample Object Independent	2.00×10^{-4}
Section #3	2.36×10^{-5}	Sample Object Copula Dependent	8.00×10^{-4}

Clearly, both wind load and wave load act on the sections #2 (column) of the sample object. The failure probability considering dependent loads (the dependence between the parameters to calculate the environmental loads is defined in Step 3) should be addressed by the copula-based bivariate failure function in Equation (3.13). On the contrary, the failure probability assuming independent loads is calculated by the bivariate lognormal distribution with correlation coefficient ρ equals to 0.

$$BFF(P_1, P_2) = f_1(P_1) \times f_2(P_2) \times c(F_1(P_1), F_2(P_2)) \quad (3.13)$$

Where $\mathrm{BFF}(\mathrm{P}_1, \mathrm{P}_2)$ is the bivariate failure density function, P_1 and P_2 are parameters to calculate wind loads and wave loads, $f(P)$ is the load calculation model and physical reliability model, and $\mathrm{c}(\mathrm{F}_1(P_1), F_2(P_2))$ is the copula-based dependence function.

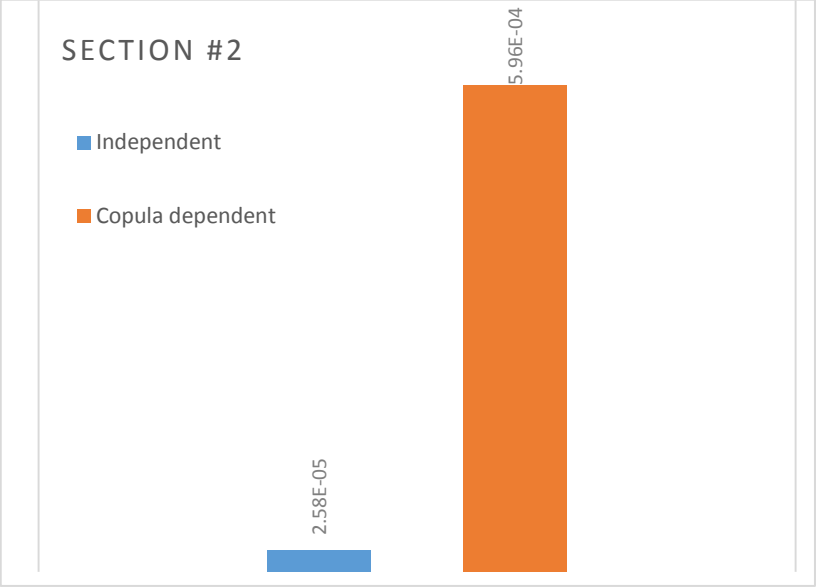

Figure 3-7. Failure probability of section #2 (column) with dependent and independent loads

The failure probabilities of the components and the sample object are presented in Table 3-4. The failure probabilities of section #2 of the column are shown in Figure 3-7. The failure probability considering dependent loads is greater than the failure probability with independent loads assumption. It is calculated in Step 3 that the dependence between the wind speed and wave height for the example data sample is established by the Gumbel copula. The results reveal that the failure probability estimated considering independent environmental loads is an underestimation. It is therefore crucial to take dependence into consideration to provide a safety operational envelope using the copula-based bivariate failure function.

3.3 Application of the proposed methodology

The proposed methodology is applied to a typical semi-submersible mobile unit (SMU) operating in the Grand Banks to identify a safety operating envelope. The results are compared with the traditional approach.

3.3.1 Steps 1-2: Real-time weather observation and environmental load calculation

In this paper, 1000 sets of wave data and concurrent meteorological observation data from the buoy: Banquereau – 44139 are used from the wave data available on-line from the Department of Fisheries and Oceans Canada (DFO) [15]. Figure 3-8 presents the wind speed and wave height observed from Banquereau – 44139.

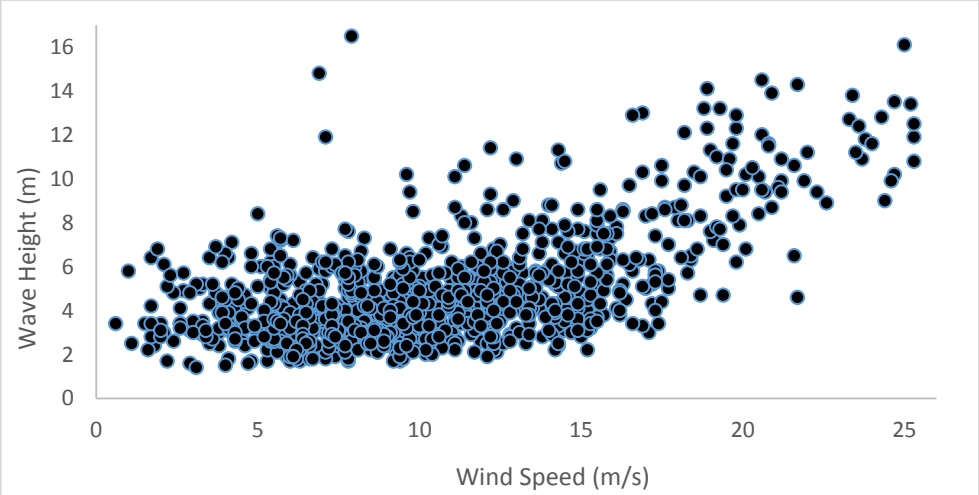

Figure 3-8. Scatter plot of wind speed and wave height for Banquereau – 44139

As the basis of the proposed modelling, it is necessary to clarify the geometric

dimension parameters and related operational characteristics of the SMU. Table 3-5 shows the physical characteristics of the SMU.

Table 3-5 Physical characteristics of the SMU

Component	Parameter	Value	Component	Parameter	Value
Derrick	Height	60 m		Height	8 m
Deck	Height	8 m	Pontoon	Length	60 m
Column	Height	24 m		Width	20 m
	Diameter	12 m	Waterline	Depth	16 m
Winds	Maximum	50 m/s	Waves	Maximum	35 m

As revealed in Figure 3-9, the primary structural components from the top to the bottom for the typical SMU are the derrick, deck, columns, and pontoons. The derrick and columns are divided into three sections according to the height. Similarly, sections #1, #2 and #3 of the pontoon are generated by the length. Then, the wind-induced loads and wave-induced loads for each section are calculated from the wind load modeling and Morison load model, as suggested from DNVGL-RP-C205 [3].

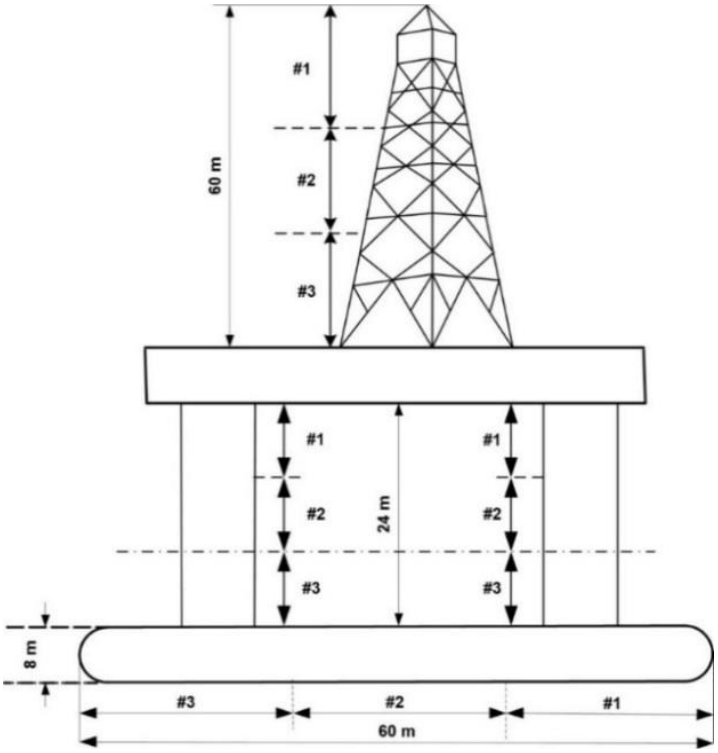

Figure 3-9. Schematic of the typical SMU with generated sections

3.3.2 Step 3: Define dependence calculated using data in Step 1

The crux of the proposed methodology is to deduce the dependence function between the parameters to calculate the environmental loads. In practical situations, the occurrence of the surge is usually related to extreme wind. Hence, it is of considerable significance to consider the dependence to construct the bivariate failure function.

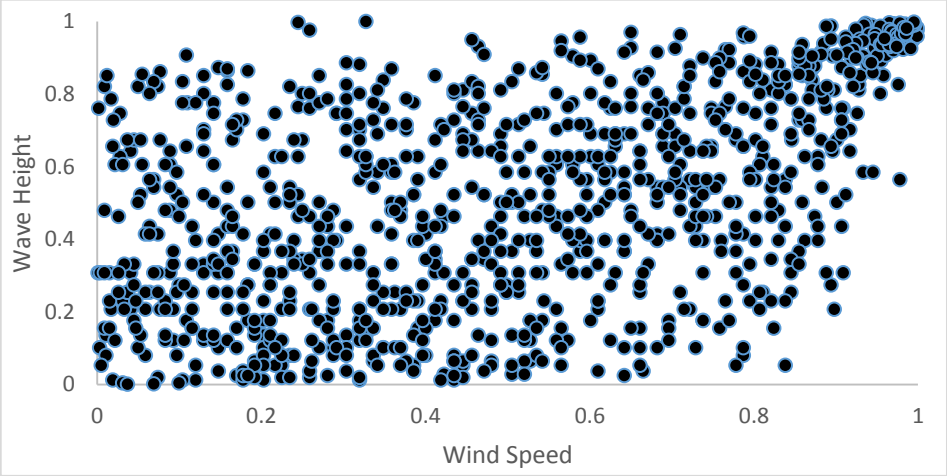

Figure 3-10. Scatter plot of wind speed and wave height after uniform transformation for Banquereau – 44139

Following the rescaled empirical distribution function in Equation (3.7), the uniform transformed marginals of wind speed and wave height are shown in Figure 3-10. To describe the dependence structure to the greatest extent possible, three copula models from the Archimedean family are filtered out as potential candidates for their ability to reflect lower tail dependence, radial symmetry, and upper tail dependence.

Table 3-6 CML and model selection calculation results for 1000 sets of data from the buoy: Banquereau – 44139

Copula	$\boldsymbol{\delta}$	$\boldsymbol{LLF(\delta)}$	**AIC**	Δ_i	$\boldsymbol{w_i}$
Clayton	0.498	57.591	-113.182	284.378	0
Frank	3.475	138.265	-274.530	123.030	0
Gumbel	1.573	199.780	-397.560	0.000	1

Then, the uniform marginals are substituted into the copula density, which is processed using MATLAB. The dependence parameters δ are calculated using maximum likelihood estimation with Equation (3.8). Afterward, the AIC value, AIC difference Δ_i and Akaike weights w_i are presented in Table 3-6.

In view of the best model selection criteria, convincing evidence is shown that the Gumbel copula is the closest model to the true model. Generally speaking, the larger AIC difference Δ_i is, the smaller the Akaike weight w_i is, and the farther the distance between the candidate model and the true model. Based on the rules of thumb proposed by Burnham and Anderson [21], the level of support for the candidate model is essentially none if $\Delta_i$is larger than 10. The Gumbel copula is selected to describe the dependence structure between the parameters to calculate the environmental loads. It is also apparent from Figure 3-8 and Figure 3-10 that the occurrence of strong winds is always accompanied with rogue waves. In summary, the upper tail dependence between the wind speed and wave height is captured by the Gumbel copula.

3.3.3 Step 4-5: Failure probability calculation and comparison

As mentioned before, the main structural components of the SMU include the derrick, deck, columns and pontoons. The derrick raises and lowers drilling tools, while the deck stores the generator room, machine equipment and so on. Due to the support of columns that connect the deck and pontoons (the sources of the

floatation), the SMU is a column-stabilized mobile unit.

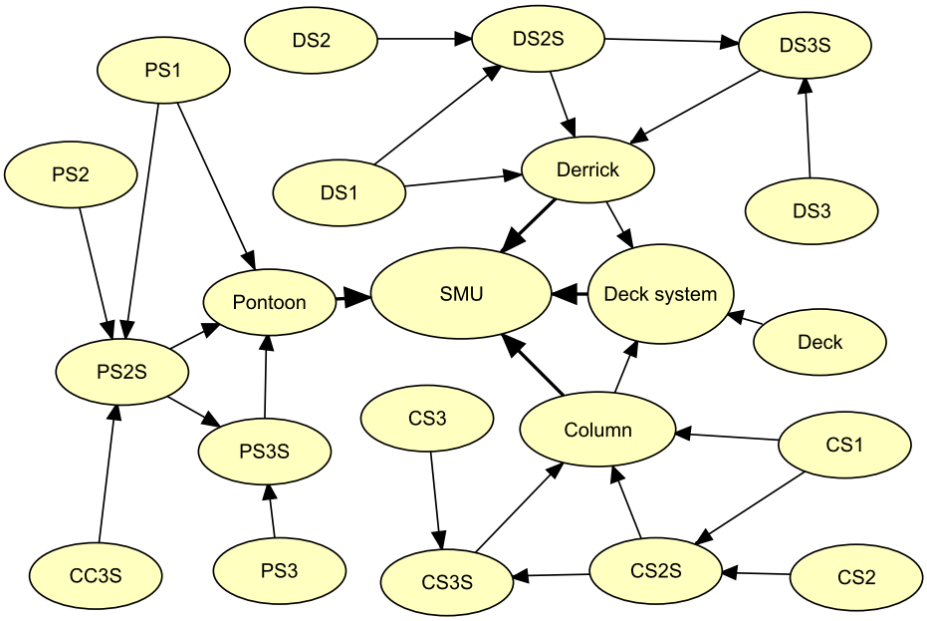

Figure 3-11. Tailored BN for the SMU

Consequently, the construction of the BN follows the unit configuration logic as shown in Figure 3-11 . In general, the tailored BN consists of four parts, which illustrate the four subsystems: the pontoon, column, derrick, and deck. As shown in Figure 3-9 , the pontoon, column and derrick have three sections, which are represented as PS1 – 3, CS1 – 3, and DS1 – 3 in the BN. Apart from the necessary sections, the mutual dependences are considered as distinguished with the suffix "S". Due to the fact that falling debris may destroy the adjacent sections, the lower sections suffer damage from environmental loads directly and debris from adjacent higher sections. The damage dependences are adopted from the CPTs in Fu's research [26]. Without the stabilization of the columns, the deck could not bear the derrick. In addition, falling debris from the derrick may hit the deck, which would further threaten the integrity of the deck. The subsystem of the

pontoon is responsible for floatation. Accordingly, failure of any one of the abovementioned components would result in the failure of the SMU.

To display the advantage of the operational failure assessment for the SMU considering dependent environmental loads, a comparison study is conducted using one sample of data (wind speed $25\ \mathrm{m/s}$, wave height $16.1\ \mathrm{m}$) as a case example. The maximum bearable environmental loads for the SMU are calculated with the design and manufactured maximum allowable parameters: wind speed $50\ \mathrm{m/s}$, wave height $35\ \mathrm{m}$. It is recommended by DNVGL-OS-C101 [23] that the corresponding failure probabilities be 10^{-2}. For the sake of simplicity, the CVs for the sections impacted by combined environmental loads are assumed as 0.295 for the wave load resistances and 0.222 for the wind load resistances. Table 3-7 shows the results of the maximum bearable environmental loads and the case example loads for the SMU.

As can be seen, sections #1 and #2 of the column are impacted by wind loads and wave loads simultaneously using the example case data. The copula-based bivariate failure function as expressed in Equation (3.13) is used to calculate the failure probability considering dependent loads. For the purpose of comparison, the failure probability assuming the independent loads is solved by the joint bivariate lognormal distribution ($\rho = 0$). In brief, the probabilities of the nodes in the Bayesian network are summarized in Table 3-8 . The comparison results are shown in Figure 3-12.

3.4 Results and Discussion

Table 3-7 shows that the actual environmental loads are less than the maximum

bearable loads because of the small wind speed and low wave height. Following this, the failure probabilities in Table 3-8 reveal that the SMU operates within the bounds of safety permission under the circumstances of wind speed $25\ \mathrm{m/s}$ and wave height $16.1\ \mathrm{m}$, as the corresponding failure probability is merely 3.00×10^{-4}. The failure probability for the component derrick is 7.75×10^{-5} under the impact of wind load only. The failure probabilities of the column and pontoon are 7.74×10^{-5} and 8.02×10^{-5}, respectively, which are nearly at the same magnitude.

Table 3-7 Environmental loads for the SMU

Structure Level		Maximum Bearable Loads		Case Example loads	
Component	Section Number	Wind 10^3 Pa	Wave 10^4 Pa	Wind 10^2 Pa	Wave 10^4Pa
Derrick	#1	3.34	-	8.36	-
	#2	3.10	-	7.74	-
	#3	2.77	-	6.92	-
Deck	-	2.44	13.8	6.10	-
Column	#1	2.15	7.02	5.38	4.53
	#2	1.58	5.99	3.95	4.07
	#3	-	5.11	-	3.35
Pontoon	#1	-	7.74	-	4.58
	#2	-	7.74	-	4.58

	#3	-	7.74	-	4.58

However, Figure 3-12 demonstrates the superiority of assessing the load impact on the failure of the system considering the dependence among parameters to calculate environmental loads. As is shown in Figure 3-12, the failure probabilities of sections #1 and #2 calculated by the copula-based bivariate failure function are approximately fifty times larger than the one with the independent loads assumption. The failure probability of the SMU is integrated with the aid of the BN. Consequently, the failure probability of the SMU considering dependent loads is 10 times greater than the one without taking dependence into account (ρ = 0).

Table 3-8 Nodes probabilities of the Bayesian network

Node	Probability	Node	Probability
Derrick	7.75×10^{-5}	Section #2 Independent	2.77×10^{-5}
Section #1	2.66×10^{-5}	Section #2 Copula Dependent	1.42×10^{-3}
Section #2	2.53×10^{-5}	Section #3	2.31×10^{-5}
Section #3	2.56×10^{-5}	Pontoon	8.02×10^{-5}
Deck	2.60×10^{-5}	Section #1	2.26×10^{-5}
Column Independent	7.74×10^{-5}	Section #2	2.26×10^{-5}

Column Copula Dependent	2.80×10^{-3}	Section #3	2.26×10^{-5}
Section #1 Independent	2.66×10^{-5}	SMU Independent	3.00×10^{-4}
Section #1 Copula Dependent	1.36×10^{-3}	SMU Copula Dependent	3.20×10^{-3}

Under practical circumstances, the occurrence of strong winds tends to be accompanied with severe wave conditions. Thus, the marginal failure probabilities induced by the large wind loads are often accompanied by high failure probabilities brought by the significant wave loads for the system under the impact of the combined environmental loads. Therefore, the joint failure probability estimated by the copula-based bivariate failure function turns out to be more realistic, as it captures the dependence details between the parameters to calculate environmental loads.

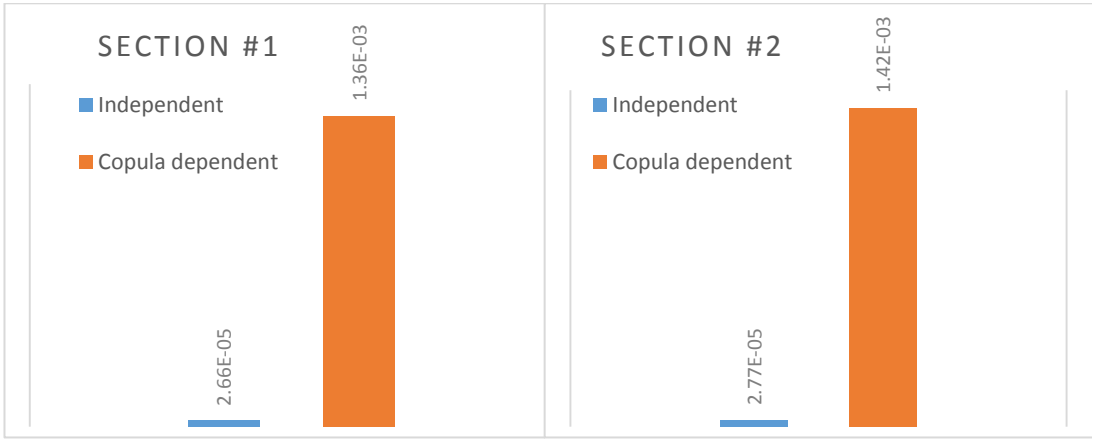

Figure 3-12. Failure probabilities of section #1 and section #2 of the column with dependent loads and independent loads

On the other hand, Figure 3-10 and the selected Gumbel copula show the upper tail dependence character. This clearly shows that the stronger wind speed and higher wave height have more substantial dependence. On the basis of the copula-based bivariate failure function in Equation (3.13), the larger the dependency, the greater the value of the failure probability. Therefore, it is vital to take dependence into consideration in extreme weather conditions.

In conclusion, consideration of the dependence structure between the parameters to calculate the environmental loads for operational failure assessment is necessary for the sake of safety production, especially in harsh environments. It allows the failure probability to be much closer to reality. If feasible, it is recommended that the historical wave and meteorological data of the operational location be thoroughly investigated.

3.5 Conclusions

This paper proposes a novel methodology and robust model that consider real-time weather observation and estimate the operational failure probability of the system. The methodology is explained with a simple example. The developed robust model is tested and applied to a detailed case study. The novelty of this paper is the consideration of dependence between the parameters to calculate environmental loads. The dependence is considered using the copula-based bivariate failure function. The dependence parameters are estimated by maximizing the pseudo log-likelihood functions. The selection of the best model among all candidate copula models is accomplished with the aid of Akaike's

information criterion (AIC). AIC differences and Akaike weight measure the distances between the best model and candidate model and the level of empirical support.

The comparison of the proposed approach with the traditional approach considering independence demonstrates the advantage of the operational failure assessment model considering the copula function. The failure probability considering dependent loads calculated by the copula-based bivariate failure function is noticeably higher and closer to the real-life situation. This observation emphasizes the vital significance of considering dependence when defining safe operation envelopes under extreme weather conditions. This work will help decision-makers make informed operational decisions for the system.

It is important to note that one copula may not define all environmental parameter conditions. The accuracy of copula selection strongly depends on the set of data (in terms of the frequency and broader range). It is recommended that a proper copula function be defined considering a wide range of data so both temporal and spatial variations are captured in defining the dependency.

3.6 References

[1] Beven, J. L., Avila, L. A., Blake, E. S., Brown, D. P., Franklin, J. L., Knabb, R. D., ... & Stewart, S. R. (2007). Annual summary: Atlantic hurricane season of 2005. Monthly Weather Review, 136, 1109-1173.

[2] Cruz, A. M., & Krausmann, E. (2008). Damage to offshore oil and gas facilities following hurricanes Katrina and Rita: An overview. Journal of Loss Prevention in the Process Industries, 21(6), 620-626.

[3] DNVGL-RP-C205, Enviromental conditions and enviromental loads. August 2017. DNV GL

[4] American Bureau of Shipping (ABS), Rules for building and Classing Mobile Offshore Drilling Units. 2019

[5] Suja-Thauvin, L., Krokstad, J. R., & Bachynski, E. E. (2018). Critical assessment of non-linear hydrodynamic load models for a fully flexible monopile offshore wind turbine. Ocean Engineering, 164, 87-104.

[6] Caille, F, Bozonnet, P, Melis, C, Poirette, Y, Perdrizet, P (2017). Model test and simulation comparison for an inclined-leg TLP dedicated to floating wind. Paper Presented at the ASME 2017 36th International Conference on Ocean, Offshore and Arctic Engineering. San Francisco, CA, USA,

[7] Flis, L. (2016). Application of the rules of the American Bureau of Shipping (ABS) to design mobile offshore structures. Scientific Journal of Polish Naval Academy, 205(2), 17-28.

[8] Li, D. J., Fu, Q., Du, Z. F., Xiao, Y., Han, R. G., & Sun, H. H. (2018). Structural Configuration Selection and Optimization of 7th Generation Semi-Submersible Drilling Unit. Paper presented at the ASME 2018 37th

International Conference on Ocean, Offshore and Arctic Engineering. Madrid, Spain.

[9] Durante, F., Sempi, C. (2015), Principles of Copula Theory, CRC Press, Boca Raton, FL.

[10] Jia, X., Xing, L., & Li, G. (2018). Copula‐based reliability and safety analysis of safety‐critical systems with dependent failures. Quality and Reliability Engineering International, 34(5), 928-938.

[11] Zhang, X., & Wilson, A. (2017). System reliability and component importance under dependence: A copula approach. Technometrics, 59(2), 215-224.

[12] Hashemi, S. J., Ahmed, S., & Khan, F. (2015). Operational loss modelling for process facilities using multivariate loss functions. Chemical Engineering Research and Design, 104, 333-345.

[13] Guo, C., Khan, F., & Imtiaz, S. (2019). Copula-based Bayesian network model for process system risk assessment. Process Safety and Environmental Protection, 123, 317-326.

[14] Shen, L., Zhang, Y., & Zhuang, X. (2016). Research on Function Reliability of Gear Door Lock System with Correlated Failure Models Based on Mixed Copula. Paper Presented at the ASME 2016 International Mechanical Engineering Congress and Exposition. American Society of Mechanical Engineers. Phoenix, Arizona, USA.

[15] Department of Fisheries and Oceans Canada (DFO). Wave data available on-line. Available online: http://isdm-gdsi.gc.ca/isdm-gdsi/waves-vagues/data-donnes/data-donnees-eng.asp?medsid=C44139.(accessed on

05 September 2019).

[16] Sklar, M. (1959). Fonctions de repartition an dimensions et leurs marges. Publ. inst. statist. univ. Paris, 8, 229-231.

[17] Nelsen, R.b., (2006). An introduction to Copulas, second ed. Springer, New York, NY.

[18] Melo, R., Accioly, S., & Aiube, F. A. L. (2008). Analysis of crude oil and gasoline prices through copulas. Cadernos do IME-Série Estatística, 24(1), 15.

[19] Genest, C., & Favre, A. C. (2007). Everything you always wanted to know about copula modeling but were afraid to ask. Journal of hydrologic engineering, 12(4), 347-368.

[20] MathWorks, 2017. MATLAB Release 2017b. The MathWorks, Inc., Natick, Massachusetts, United States.

[21] Burnham, K. P., Anderson, D. R., (2002). Model Selection and Multi-Model Inference: A Practical Information-Theoretic Approach, 2nded. Springer, Secaucus, NJ, USA.

[22] Ebeling CE. (1997) An Introduction to Reliability and Maintainability Engineering.2nd ed. New Delhi: McGraw Hill;

[23] DNVGL-OS-C101, Design of offshore steel structures, general - LRFD method. July 2019. DNV GL

[24] Zhang, S. (2017, August 25). When a hurricane hits an offshore oil platform: Harvey could seriously damage oil and gas operations in the Gulf of Mexico. The Atlantic: Science Edition. Retrieved from: https://www.theatlantic.com /science/archive/2017/08/harvey-offshore-

platform-oil-gas/537960/

[25] Yuan, Z., Khakzad, N., Khan, F., & Amyotte, P. (2015). Risk analysis of dust explosion scenarios using Bayesian networks. Risk analysis, 35(2), 278-291.

[26] Fu, J., & Khan, F. (2019). Operational failure model for semi-submersible mobile units in harsh environments. Ocean Engineering, 191, 106332.

Chapter 4. Summary

Keeping the safety operation of the offshore facilities in the harsh environment is the top priority in meeting the growing demand for energy. Therefore, this thesis proposes two related methodologies that assess the operational risk quantitatively with combined environmental loads considering the dependence structure between the real-time environmental parameters.

Chapter 1 introduces the overview of the current models that are employed to capture the dynamic response of the offshore facilities under extreme weather conditions and researchers' application using related standards recommended by classification societies to calculate environmental loads.

Chapter 2 presents a novel model that defines the operational failure envelope for decision-makers' reference which applies the weather condition and physical characteristics of the offshore facilities.

Chapter 3 proposes a robust copula-based bivariate operational failure assessment model which aims to explore the influence of the dependence function among parameters to calculate the environmental loads.

Chapter 4 concludes the research, illustrates the novelty and highlights the contribution of the developed methodologies. In the end, further recommendations and future work are presented here for the sake of improvement.

4.1 Conclusions

Previous popular evaluation indicators mainly focus on either external hydrodynamic performance or internal structure dynamic analysis instead of quantitatively analyzing the operational risk. Furthermore, the dependencies among parameters to calculate environmental loads are ignored which

underestimates the impact on the failure of the system. Therefore, this work fills in the research gaps by assessing the operational risk quantitatively with combined environmental loads which consider the dependency function.

The physical reliability model and the BN are used for the operational failure model which is verified with a catastrophe capsizing accident - the Ocean Ranger as a case application. The proposed model applies the weather conditions on-site and the unit configuration and estimates a very high probability of failure which predicts a dangerous prevailing situation. The occurrence of the fateful event confirms the accuracy and effectiveness. It is demonstrated that the proposed anticipated risk estimation model is a reliable tool to develop and monitor an operational failure envelope of the SMU in given environmental conditions.

The copula-based bivariate operational failure assessment model is validated by a typical semi-submersible mobile unit (SMU) operating in the Grand Banks with the obtained wave and concurrent meteorological observation data from the buoy: Banquereau – 44139. The comparison study of the proposed approach with the traditional approach considering independence demonstrates the advantage of the operational failure assessment model which takes the copula function into account. The obvious differences indicate that the proposed model which captures the dependence details among parameters to calculate the environmental loads is able to better guide policy-makers for safety operational decisions.

4.2 Recommendation

It is worth mentioning that the environmental loads acting on the offshore facilities are not only limited to the wind and wave loads under the practical situation. More complicated and considerable cases such as currents and sea ice

induced loads should be taken into consideration to extend the operational disturbance to a broader scope of contexts.

The following aspects for further research can achieve a deeper insight into the copula-based bivariate failure model. It is important to note that the accuracy and precision of copula selection strongly depend on the data set. The broader range the data sets, the more the dependence details can be reflected. It is recommended that the proper copula function be defined considering a wide range of data, so both temporal and spatial variations are captured in defining the dependency. Therefore, the further research direction is to determine the suitable copula function facing the widely encountered issue of data paucity.